Contemporary Mathematics

hp–Version Discontinuous Galerkin Methods with Interior Penalty for Partial Differential Equations with Nonnegative Characteristic Form

Kathryn Harriman, Paul Houston, Bill Senior, and Endre Süli

Abstract. In this paper we consider the *a posteriori* and *a priori* error analysis of *hp*–discontinuous Galerkin interior penalty methods for second–order partial differential equations with nonnegative characteristic form. In particular, we discuss the question of error estimation for linear target functionals, such as the outflow flux and the local average of the solution. Based on our *a posteriori* error bound we design and implement the corresponding adaptive algorithm to ensure reliable and efficient control of the error in the prescribed functional to within a given tolerance. This involves exploiting both local polynomial-degree variation and local mesh subdivision. The theoretical results are illustrated by a series of numerical experiments.

1. Introduction

Discontinuous Galerkin finite element methods (DGFEMs, for short) date back to the early 1970's; they were simultaneously proposed by Reed & Hill [**22**] in 1973 for the numerical solution of the neutron transport equation and by Nitsche [**18**] in 1971 as nonstandard schemes for the approximation of second–order elliptic equations. Since then extensive work has been devoted to the development and analysis of these methods for a wide range of applications; for a recent survey and historical review, we refer to the article by Cockburn *et al.* [**8**]. One of the key advantages of the DGFEM in comparison with standard Galerkin finite element methods based on continuous piecewise polynomials is their high degree of locality. Indeed, the computational stencil of the DGFEM remains very compact, even as the degree of the approximating polynomial is increased. Thereby, high–order adaptive *hp*– and spectral element approximations may be handled in a particularly flexible and simple manner. This class of adaptive finite element methods offers tremendous gains in computational efficiency in comparison with standard mesh refinement algorithms which only incorporate local *h*–refinement with a given (fixed) polynomial

1991 *Mathematics Subject Classification.* 65N12, 65N15, 65N30.

Key words and phrases. Adaptivity, *hp*–finite element methods, discontinuous Galerkin methods, PDEs with nonnegative characteristic form.

The authors acknowledge the financial support of the EPSRC (Grant Numbers: GR/R17041 for KH and ES and GR/N24230 for PH and BS).

degree. For a recent review of hp–refinement strategies, we refer to [**14**]; see also [**1, 4, 16, 23, 25**] for related work.

In the series of papers [**13, 14, 16, 25, 26**], we have developed so–called 'goal–oriented' *a posteriori* error estimation for hp–adaptive DGFEMs applied to first–order hyperbolic conservation laws; see also [**10**] and the article of Larson & Barth [**17**] in the case of the h–version of the DGFEM. Here, in contrast to traditional *a posteriori* error estimation which seeks to bound the error with respect to a given norm, goal–oriented *a posteriori* error estimation bounds the error measured in terms of certain target functionals of real or physical interest. Typical examples include the mean value of the field over the computational domain Ω, the normal flux through the outflow boundary of Ω and the evaluation of the solution at a given point in Ω. For related work, we refer to Becker & Rannacher [**7**].

The purpose of this paper is to extend our earlier work on first–order hyperbolic problems to a general class of second–order partial differential equations with nonnegative characteristic form. For the discretization of the leading order terms, we employ a class of interior penalty methods which lead to either a symmetric or nonsymmetric discretization of the diffusive operator, depending on the choice of a given parameter within the scheme; in the following we write SIP/NIP to denote the symmetric/nonsymmetric versions of the interior penalty method, respectively. While a symmetric discretization of a self–adjoint operator seems quite natural, the NIP scheme is often preferred, particularly for advection–dominated problems where the underlying discretization matrix is nonsymmetric anyway, as it is stable for any choice of a certain discontinuity–penalization parameter $C_\sigma > 0$, cf. [**2, 12, 21**], for example; see also Theorem 3.1 below. On the other hand, the SIP scheme is only stable when $C_\sigma > 0$ is chosen sufficiently large. In terms of accuracy, both schemes converge at the optimal rate when the error is measured in terms of the energy norm, but the lack of adjoint consistency, cf. [**2**], of the NIP method leads to suboptimal convergence of the error when measured in terms of the L_2 norm. In this case, the SIP scheme is still optimally convergent, while the NIP method is suboptimal by a full order; however, numerical experiments indicate that in practice the L_2 norm of the error arising from the NIP scheme converges to zero at the optimal rate when the polynomial degree p is odd, cf. [**12**]. Thereby, in practice the loss of optimality of the NIP scheme when the error is measured in terms of the L_2 norm only arises for even p. In this article, however, we shall show that the lack of adjoint consistency of the NIP scheme leads to suboptimal rates of convergence for all $p \geq 2$, when the error is measured in terms of a certain (linear) target functional $J(\cdot)$ of practical interest, such as $J : v \mapsto \int_\Omega v(x)\psi(x)\,\mathrm{d}x$, for example, where ψ is a given weight-function. More precisely, for fixed p we shall show that the error measured in terms of $J(\cdot)$ behaves like $\mathcal{O}(h^{2p})$ when the SIP scheme is employed, while for the NIP scheme, we only have the rate of convergence $\mathcal{O}(h^p)$ as h tends to zero. For related work on *a posteriori* error estimation for DGFEMs with interior penalty, see Becker *et al.* [**5, 6**] and Rivière & Wheeler [**23**], for example.

The paper is structured as follows. In Section 2 we introduce the model problem and formulate its discontinuous Galerkin finite element approximation. Then, in Sections 3 and 4 we develop the *a posteriori* and *a priori* error analyses of the error measured in terms of certain linear target functionals of practical interest.

Our *a posteriori* error bounds stem from a duality argument and include computable residual terms multiplied by local weights involving the dual solution; cf. [**7, 10, 16, 25**]. Guided by our *a posteriori* error analysis, in Section 5 we design an hp–adaptive finite element algorithm to guarantee reliable and efficient control of the error in the computed functional to within a fixed user–defined tolerance. The performance of the resulting hp–refinement strategy is then studied in Section 6 through a series of numerical experiments. In particular, we demonstrate the superiority of using hp–adaptive mesh refinement over the traditional h–refinement method, where the degree of the approximating polynomial is kept fixed at some low value. Finally, in Section 7 we summarize the work presented in this paper and draw some conclusions.

2. Model problem and discretization

Let Ω be a bounded open polyhedral domain in $\mathbb{R}^d$, $d \geq 2$, and let Γ signify the union of its $(d-1)$–dimensional open faces. We consider the advection–diffusion–reaction equation

$$\mathcal{L}u \equiv -\nabla \cdot (a\nabla u) + \nabla \cdot (\mathbf{b}u) + cu = f \ , \tag{2.1}$$

where $f \in L_2(\Omega)$ and $c \in L_\infty(\Omega)$ are real–valued, $\mathbf{b} = \{b_i\}_{i=1}^d$ is a vector function whose entries b_i are Lipschitz continuous real–valued functions on $\bar{\Omega}$, and $a = \{a_{ij}\}_{i,j=1}^d$ is a *symmetric* matrix whose entries a_{ij} are bounded, piecewise continuous real–valued functions defined on $\bar{\Omega}$, with

$$\boldsymbol{\zeta}^{\mathrm{T}} a(x)\boldsymbol{\zeta} \geq 0 \quad \forall \boldsymbol{\zeta} \in \mathbb{R}^d \, , \quad \text{a.e. } x \in \bar{\Omega} \ . \tag{2.2}$$

Under this hypothesis, (2.1) is termed a *partial differential equation with nonnegative characteristic form*. By $\mathbf{n}(x) = \{n_i(x)\}_{i=1}^d$ we denote the unit outward normal vector to Γ at $x \in \Gamma$. On introducing the so called *Fichera function* $\mathbf{b} \cdot \mathbf{n}$ (cf. [**20**]), we define

$$\Gamma_0 = \left\{ x \in \Gamma : \ \mathbf{n}(x)^{\mathrm{T}} a(x)\mathbf{n}(x) > 0 \right\} ,$$

$$\Gamma_- = \{ x \in \Gamma \backslash \Gamma_0 : \ \mathbf{b}(x) \cdot \mathbf{n}(x) < 0 \} \ , \quad \Gamma_+ = \{ x \in \Gamma \backslash \Gamma_0 : \ \mathbf{b}(x) \cdot \mathbf{n}(x) \geq 0 \} \ .$$

The sets Γ_- and Γ_+ will be referred to as the inflow and outflow boundary, respectively. Evidently, $\Gamma = \Gamma_0 \cup \Gamma_- \cup \Gamma_+$. If Γ_0 is nonempty, we shall further divide it into disjoint subsets Γ_{D} and Γ_{N} whose union is Γ_0, with Γ_{D} nonempty and relatively open in Γ. We supplement (2.1) with the boundary conditions

$$u = g_{\mathrm{D}} \quad \text{on} \quad \Gamma_{\mathrm{D}} \cup \Gamma_- \ , \qquad \mathbf{n} \cdot (a\nabla u) = g_{\mathrm{N}} \quad \text{on} \quad \Gamma_{\mathrm{N}} \ , \tag{2.3}$$

and adopt the (physically reasonable) hypothesis that $\mathbf{b} \cdot \mathbf{n} \geq 0$ on Γ_{N}, whenever Γ_{N} is nonempty. Additionally, we assume that the following (standard) positivity hypothesis holds: there exists a constant vector $\boldsymbol{\xi} \in \mathbb{R}^d$ such that

$$c(x) + \frac{1}{2} \nabla \cdot \mathbf{b}(x) + \mathbf{b}(x) \cdot \boldsymbol{\xi} > 0 \ \text{ a.e. } \ x \in \Omega \ . \tag{2.4}$$

For simplicity of presentation, we assume throughout that (2.4) is satisfied with $\boldsymbol{\xi} \equiv \mathbf{0}$; we then define the positive function c_0 by

$$(c_0(x))^2 = c(x) + \frac{1}{2} \nabla \cdot \mathbf{b}(x) \ \text{ a.e. } \ x \in \Omega \ . \tag{2.5}$$

For the well-posedness theory of the boundary value problem (2.1), (2.3), in the case of homogeneous boundary conditions, we refer to [**12**] (see also [**15**]).

2.1. Meshes, finite element spaces and traces. We consider shape–regular meshes $\mathcal{T}_h = \{\kappa\}$ that partition the domain Ω into open element domains κ, with possible hanging nodes. For the sake of simplicity, we shall suppose that the mesh is 1-irregular in the sense that there is at most one hanging node per element-face which we assume to be the barycenter of the face. We denote by h the piecewise constant mesh function with $h(x) \equiv h_\kappa = \mathrm{diam}(\kappa)$ when x is in element κ. We assume that each $\kappa \in \mathcal{T}_h$ is a smooth bijective image of a fixed reference element $\hat{\kappa}$, that is, $\kappa = F_\kappa(\hat{\kappa})$ for all $\kappa \in \mathcal{T}_h$, where $\hat{\kappa}$ is either the open unit simplex

$$\hat{\kappa}_{\mathrm{S}} = \{\hat{x} = (\hat{x}_1, \ldots, \hat{x}_d) \in \mathbb{R}^d \,:\, 0 < x_1 + \cdots + x_d < 1,\ x_i > 0,\ i = 1, \ldots, d\}$$

or the open hypercube $\hat{\kappa}_{\mathrm{C}} = (-1, 1)^d$ in $\mathbb{R}^d$. On $\hat{\kappa}$ we define spaces of polynomials of degree $p \geq 1$ as follows:

$$\mathcal{Q}_p = \mathrm{span}\,\{\hat{x}^\alpha : 0 \leq \alpha_i \leq p,\ \ 1 \leq i \leq d\}\,, \quad \mathcal{P}_p = \mathrm{span}\,\{\hat{x}^\alpha : 0 \leq |\alpha| \leq p\}\,.$$

To each $\kappa \in \mathcal{T}_h$ we assign an integer $p_\kappa \geq 1$; collecting the p_κ and F_κ in the vectors $\mathbf{p} = \{p_\kappa : \kappa \in \mathcal{T}_h\}$ and $\mathbf{F} = \{F_\kappa : \kappa \in \mathcal{T}_h\}$, respectively, we introduce the finite element space

$$\begin{aligned} S^{\mathbf{p}}(\Omega, \mathcal{T}_h, \mathbf{F}) \quad = \quad & \{u \in L_2(\Omega) \,:\, u|_\kappa \circ F_\kappa \in \mathcal{Q}_{p_\kappa} \text{ if } F_\kappa^{-1}(\kappa) = \hat{\kappa}_{\mathrm{C}} \\ & \text{and} \quad u|_\kappa \circ F_\kappa \in \mathcal{P}_{p_\kappa} \text{ if } F_\kappa^{-1}(\kappa) = \hat{\kappa}_{\mathrm{S}};\ \kappa \in \mathcal{T}_h\}\,. \end{aligned}$$

Associated with $\mathcal{T}_h$, we introduce the broken Sobolev space of composite order $\mathbf{s}$ defined by

$$H^{\mathbf{s}}(\Omega, \mathcal{T}_h) = \{u \in L_2(\Omega) :\ u|_\kappa \in H^{s_\kappa}(\kappa) \quad \forall \kappa \in \mathcal{T}_h\}\,,$$

equipped with the broken Sobolev norm and corresponding seminorm, respectively,

$$\|u\|_{\mathbf{s},\mathcal{T}_h} = \Big(\sum_{\kappa\in\mathcal{T}_h} \|u\|^2_{H^{s_\kappa}(\kappa)}\Big)^{1/2}, \qquad |u|_{\mathbf{s},\mathcal{T}_h} = \Big(\sum_{\kappa\in\mathcal{T}_h} |u|^2_{H^{s_\kappa}(\kappa)}\Big)^{1/2}. \tag{2.6}$$

When $s_\kappa = s$ for all $\kappa \in \mathcal{T}_h$, we write $H^s(\Omega, \mathcal{T}_h)$, $\|u\|_{s,\mathcal{T}_h}$ and $|u|_{s,\mathcal{T}_h}$. For $u \in H^1(\Omega, \mathcal{T}_h)$ we define the broken gradient $\nabla_{\mathcal{T}_h} u$ of u by $(\nabla_{\mathcal{T}_h} u)|_\kappa = \nabla(u|_\kappa)$, $\kappa \in \mathcal{T}_h$.

An *interior face* of $\mathcal{T}_h$ is defined as the (non-empty) $(d-1)$–dimensional interior of $\partial\kappa_i \cap \partial\kappa_j$, where κ_i and κ_j are two adjacent elements of $\mathcal{T}_h$, not necessarily matching. A *boundary face* of $\mathcal{T}_h$ is defined as the (non-empty) $(d-1)$–dimensional interior of $\partial\kappa \cap \Gamma$, where κ is a boundary element of $\mathcal{T}_h$. We denote by Γ_{int} the union of all interior faces of $\mathcal{T}_h$. Given a face $e \subset \Gamma_{\mathrm{int}}$, shared by the two elements κ_i and κ_j, where the indices i and j satisfy $i > j$, we write $\mathbf{n}_e$ to denote the (numbering–dependent) unit normal vector which points from κ_i to κ_j; on boundary faces, we put $\mathbf{n}_e = \mathbf{n}$. Further, for $v \in H^1(\Omega, \mathcal{T}_h)$ we define the jump of v across e and the mean value of v on e, respectively, by

$$[v] = v|_{\partial\kappa_i \cap e} - v|_{\partial\kappa_j \cap e} \quad \text{and} \quad \langle v \rangle = \frac{1}{2}\left(v|_{\partial\kappa_i \cap e} + v|_{\partial\kappa_j \cap e}\right)\,. \tag{2.7}$$

On a boundary face $e \subset \partial\kappa$, we set $[v] = v|_{\partial\kappa \cap e}$ and $\langle v \rangle = v|_{\partial\kappa \cap e}$. Finally, given a function $v \in H^1(\Omega, \mathcal{T}_h)$ and an element $\kappa \in \mathcal{T}_h$, we denote by v_κ^+ (respectively, v_κ^-) the interior (respectively, exterior) trace of v defined on $\partial\kappa$ (respectively, $\partial\kappa \backslash \Gamma$). Since below it will always be clear from the context which element κ in the subdivision $\mathcal{T}_h$ the quantities v_κ^+ and v_κ^- correspond to, for the sake of notational simplicity we shall suppress the letter κ in the subscript and write, respectively, v^+ and v^- instead.

2.2. The *hp*–discontinuous Galerkin method. Given that κ is an element in the subdivision $\mathcal{T}_h$, we denote by $\partial\kappa$ the union of $(d-1)$–dimensional open faces of κ. Let $x \in \partial\kappa$ and suppose that $\mathbf{n}_\kappa(x)$ denotes the unit outward normal vector to $\partial\kappa$ at x. With these conventions, we define the inflow and outflow parts of $\partial\kappa$, respectively, by

$$\partial_-\kappa = \{x \in \partial\kappa :\ \mathbf{b}(x)\cdot\mathbf{n}_\kappa(x) < 0\}\ ,\ \partial_+\kappa = \{x \in \partial\kappa :\ \mathbf{b}(x)\cdot\mathbf{n}_\kappa(x) \geq 0\}\ .$$

For simplicity of presentation, we suppose that the entries of the matrix a are constant on each element κ in $\mathcal{T}_h$; *i.e.*,

$$a \in \left[S^{\mathbf{0}}(\Omega,\mathcal{T}_h,\mathbf{F})\right]^{d\times d}_{\rm sym}. \tag{2.8}$$

We note that, with minor changes only, our results can easily be extended to the case of $\sqrt{a} \in [S^{\mathbf{q}}(\Omega,\mathcal{T}_h,\mathbf{F})]^{d\times d}_{\rm sym}$, where the composite polynomial degree vector $\mathbf{q}$ has nonnegative entries. In the following, we write $\bar{a} = |\sqrt{a}\,|_2^2$, where $|\cdot|_2$ denotes the matrix norm subordinate to the l_2–vector norm on $\mathbb{R}^d$ and $\bar{a}_\kappa = \bar{a}|_\kappa$; by $\bar{a}_{\tilde{\kappa}}$ we denote the arithmetic mean of the values $\bar{a}_{\kappa'}$ over those elements κ' (including κ itself) that share a $(d-1)$–dimensional face with κ.

The hp–DGFEM approximation of (2.1), (2.3) is defined as follows: find $u_{\rm DG}$ in $S^{\mathbf{p}}(\Omega,\mathcal{T}_h,\mathbf{F})$ such that

$$B_{\rm DG}(u_{\rm DG},v) = \ell_{\rm DG}(v) \tag{2.9}$$

for all $\mathbf{v} \in S^{\mathbf{p}}(\Omega,\mathcal{T}_h,\mathbf{F})$. Here, the bilinear form $B_{\rm DG}(\cdot,\cdot)$ is defined by

$$B_{\rm DG}(w,v) = B_a(w,v) + B_{\mathbf{b}}(w,v) + \theta B_e(v,w) - B_e(w,v) + B_\sigma(w,v)\,,$$

where

$$\begin{aligned}
B_a(w,v) &= \sum_{\kappa\in\mathcal{T}_h}\int_\kappa a\nabla w\cdot\nabla v\,{\rm d}x\,,\\
B_{\mathbf{b}}(w,v) &= \sum_{\kappa\in\mathcal{T}_h}\Big\{-\int_\kappa (w\,\mathbf{b}\cdot\nabla v - cwv)\,{\rm d}x\\
&\qquad + \int_{\partial_+\kappa}(\mathbf{b}\cdot\mathbf{n}_\kappa)\,w^+v^+\,{\rm d}s + \int_{\partial_-\kappa\setminus\Gamma}(\mathbf{b}\cdot\mathbf{n}_\kappa)\,w^-v^+\,{\rm d}s\Big\}\,,\\
B_e(w,v) &= \int_{\Gamma_{\rm int}\cup\Gamma_{\rm D}}\langle(a\nabla w)\cdot\mathbf{n}_e\rangle[v]\,{\rm d}s\,,\\
B_\sigma(w,v) &= \int_{\Gamma_{\rm int}\cup\Gamma_{\rm D}}\sigma[w][v]\,{\rm d}s\ ,
\end{aligned}$$

and the linear functional $\ell_{\rm DG}(\cdot)$ is given by

$$\begin{aligned}
\ell_{\rm DG}(v) &= \sum_{\kappa\in\mathcal{T}_h}\Bigg(\int_\kappa fv\,{\rm d}x - \int_{\partial_-\kappa\cap(\Gamma_{\rm D}\cup\Gamma_-)}(\mathbf{b}\cdot\mathbf{n}_\kappa)\,g_{\rm D}\,v^+\,{\rm d}s\\
&+ \int_{\partial\kappa\cap\Gamma_{\rm D}}\theta\,g_{\rm D}((a\nabla v^+)\cdot\mathbf{n}_\kappa)\,{\rm d}s + \int_{\partial\kappa\cap\Gamma_{\rm N}}g_{\rm N}v^+\,{\rm d}s + \int_{\partial\kappa\cap\Gamma_{\rm D}}\sigma g_{\rm D}v^+\,{\rm d}s\Bigg)\ .
\end{aligned}$$

Here, σ is called the *discontinuity–penalization* parameter, and is defined by

$$\sigma|_e = C_\sigma\frac{\langle\bar{a}p^2\rangle}{\langle h\rangle}\quad\text{for}\quad e\subset\Gamma_{\rm int}\cup\Gamma_{\rm D}\,, \tag{2.10}$$

where C_σ is a positive constant, cf. [**12**]. We shall adopt the convention that edges $e \subset \Gamma_{\rm int} \cup \Gamma_{\rm D}$ with $\sigma|_e = 0$ are omitted from the integrals appearing in the definition of $B_\sigma(w,v)$ and $\ell_{\rm DG}(v)$, although we shall not highlight this explicitly in our notation; the same convention is adopted in the case of integrals where the integrand contains the factor $1/\sigma$. Thus, in particular, the definition of the DG-norm, cf. (3.1) below, is meaningful even if $\sigma|_e$ happens to be equal to zero on certain edges $e \subset \Gamma_{\rm int} \cup \Gamma_{\rm D}$, given that such edges are understood to be excluded from the region of integration.

Selecting the parameter $\theta = 1$ gives rise to the so–called *Nonsymmetric Interior Penalty (NIP) method*, while setting $\theta = -1$ yields the *Symmetric Interior Penalty (SIP) scheme*.

REMARK 2.1. We remark that the formulation of the interior penalty DGFEM defined in (2.9) is referred to as the primal formulation of the scheme, cf. [**2**]. In order to see where the inter-element terms appearing in $B_{\rm DG}(\cdot,\cdot)$ and $\ell_{\rm DG}(\cdot)$ arise from, it is helpful to consider the equivalent auxiliary, or flux (cf. [**2**]) formulation. To this end, we first rewrite the advection–diffusion–reaction equation (2.1) as the following first–order system of partial differential equations:

$$\mathbf{\Phi} - a\nabla u \;=\; 0 \;\;\text{in}\;\; \Omega\,, \tag{2.11}$$

$$-\nabla\cdot\mathbf{\Phi} + \nabla\cdot(\mathbf{b}u) + cu \;=\; f \;\;\text{in}\;\; \Omega\,. \tag{2.12}$$

Taking the $L_2(\kappa)$, $\kappa \in \mathcal{T}_h$, inner product of (2.11) and (2.12) with smooth test functions τ and v, respectively, and integrating by parts gives

$$\int_\kappa \mathbf{\Phi}\cdot\tau\,{\rm d}x + \int_\kappa \nabla\cdot(a\tau)u\,{\rm d}x - \int_{\partial\kappa}(a\tau)\cdot\mathbf{n}_\kappa u\,{\rm d}s \;=\; 0\,,$$

$$\int_\kappa \mathbf{\Phi}\cdot\nabla v\,{\rm d}x - \int_{\partial\kappa\setminus\Gamma_{\rm N}} \mathbf{\Phi}\cdot\mathbf{n}_\kappa v\,{\rm d}s - \int_{\partial\kappa\cap\Gamma_{\rm N}} g_{\rm N} v\,{\rm d}s - \int_\kappa u\mathbf{b}\cdot\nabla v\,{\rm d}x + \int_{\partial\kappa}\mathbf{b}\cdot\mathbf{n}_\kappa uv\,{\rm d}s + \int_\kappa cuv\,{\rm d}x \;=\; \int_\kappa fv\,{\rm d}x\,.$$

Summing over all elements κ in the computational mesh $\mathcal{T}_h$ and introducing appropriate numerical flux functions which will be defined below, we deduce the following auxiliary formulation of the interior penalty DGFEM: find $u_h \in S^{\mathbf{p}}(\Omega,\mathcal{T}_h,\mathbf{F})$ and $\mathbf{\Phi}_h \in [S^{\mathbf{p}}(\Omega,\mathcal{T}_h,\mathbf{F})]^d$ such that

$$\sum_{\kappa\in\mathcal{T}_h}\left\{\int_\kappa \mathbf{\Phi}_h\cdot\tau\,{\rm d}x + \int_\kappa \nabla\cdot(a\tau)u_h\,{\rm d}x\right\} - \int_{\Gamma_{\rm int}\cup\Gamma_0}[(a\tau)\cdot\mathbf{n}_e]\,\widehat{u_h}\,{\rm d}s \;=\; 0\,, \tag{2.13}$$

$$\sum_{\kappa\in\mathcal{T}_h}\left\{\int_\kappa \mathbf{\Phi}_h\cdot\nabla v\,{\rm d}x - \int_\kappa (u_h\mathbf{b}\cdot\nabla v - cu_h v)\,{\rm d}x + \int_{\partial\kappa}\mathcal{H}(u_h^+,u_h^-,\mathbf{n}_\kappa)v^+\,{\rm d}s\right\}$$

$$-\int_{\Gamma_{\rm int}\cup\Gamma_{\rm D}}\widehat{\mathbf{\Phi}_h\cdot\mathbf{n}_e}\,[v]\,{\rm d}s = \sum_{\kappa\in\mathcal{T}_h}\left\{\int_\kappa fv\,{\rm d}x + \int_{\partial\kappa\cap\Gamma_{\rm N}} g_{\rm N}v\,{\rm d}s\right\} \tag{2.14}$$

for all $v \in S^{\mathbf{p}}(\Omega,\mathcal{T}_h,\mathbf{F})$ and $\tau \in [S^{\mathbf{p}}(\Omega,\mathcal{T}_h,\mathbf{F})]^d$. Here, we have employed that $\Gamma = \Gamma_{\rm D}\cup\Gamma_{\rm N}\cup(\Gamma\setminus\Gamma_0)$ and the result

$$\sum_{j=1}^d a_{ij}(x)\mathbf{n}_j = 0 \qquad \text{on}\;\Gamma\setminus\Gamma_0\,, \qquad i = 1,\ldots,d\,, \tag{2.15}$$

cf. [**15**]. The consistent and conservative (hyperbolic) numerical flux function $\mathcal{H}(u_h^+, u_h^-, \mathbf{n}_\kappa)$ is defined by

$$\mathcal{H}(u_h^+, u_h^-, \mathbf{n}_\kappa)|_{\partial\kappa} = \begin{cases} \mathbf{b}\cdot\mathbf{n}_\kappa\, g_{\mathrm{D}} & \text{when } x \in \partial_-\kappa \cap (\Gamma_{\mathrm{D}} \cup \Gamma_-)\,, \\ \mathbf{b}\cdot\mathbf{n}_\kappa\, \lim_{s\to 0^+} u_h(x - s\mathbf{b}) & \text{otherwise}\,, \end{cases}$$

for κ in $\mathcal{T}_h$, cf. Cockburn *et al.* [**8**]. For the symmetric interior penalty method, the consistent (elliptic) numerical flux functions $\widehat{u_h}$ and $\widehat{\mathbf{\Phi}_h\cdot\mathbf{n}_e}$ are defined by

$$\widehat{u_h} = \begin{cases} \langle u_h\rangle & e \subset \Gamma_{\mathrm{int}} \cup \Gamma_{\mathrm{N}}\,, \\ g_{\mathrm{D}} & e \subset \Gamma_{\mathrm{D}}\,, \end{cases}$$

and

$$\widehat{\mathbf{\Phi}_h\cdot\mathbf{n}_e} = \begin{cases} \langle (a\nabla u_h)\cdot\mathbf{n}_e\rangle - \sigma[u_h] & e \subset \Gamma_{\mathrm{int}}\,, \\ (a\nabla u_h|_e)\cdot\mathbf{n}_e - \sigma(u_h|_e - g_{\mathrm{D}}) & e \subset \Gamma_{\mathrm{D}}\,, \end{cases}$$

respectively. We note that the latter flux function is consistent for any choice of σ; however, as we shall see in the next section the stability of the underlying discretization crucially depends on the magnitude of this discontinuity–penalization parameter. For the choice of the corresponding numerical flux functions for the nonsymmetric interior penalty method, together with other schemes proposed in the literature, we refer to the article [**2**]. In order to demonstrate the equivalence of the primal and auxiliary formulations of the interior penalty DGFEM, the auxiliary variable $\mathbf{\Phi}_h$ must be eliminated from (2.13) and (2.14). This is done by selecting $\tau = \nabla v$ in (2.13), integrating by parts, and inserting the resulting expression for the term involving the dot product of $\mathbf{\Phi}_h$ and ∇v into (2.14); see [**2**] for details.

3. Stability analysis

Before embarking on the error analysis of the hp–version discontinuous Galerkin method (2.9), we first derive some preliminary results. Let us first introduce the DG–norm $|||\cdot|||_{\mathrm{DG}}$ by

$$\begin{aligned} |||w|||_{\mathrm{DG}}^2 \;=\; & \sum_{\kappa\in\mathcal{T}_h} \Big(\|\sqrt{a}\,\nabla w\|_{L_2(\kappa)}^2 + \|c_0 w\|_{L_2(\kappa)}^2 + \frac{1}{2}\|w^+\|_{\partial_-\kappa\cap(\Gamma_{\mathrm{D}}\cup\Gamma_-)}^2 \\ & + \frac{1}{2}\|w^+ - w^-\|_{\partial_-\kappa\setminus\Gamma}^2 + \frac{1}{2}\|w^+\|_{\partial_+\kappa\cap\Gamma}^2 \Big) \\ & + \int_{\Gamma_{\mathrm{int}}\cup\Gamma_{\mathrm{D}}} \sigma[w]^2\,\mathrm{d}s + \int_{\Gamma_{\mathrm{int}}\cup\Gamma_{\mathrm{D}}} \frac{1}{\sigma}\langle (a\,\nabla w)\cdot\mathbf{n}_e\rangle^2\,\mathrm{d}s\,, \end{aligned} \tag{3.1}$$

where $\|\cdot\|_\tau$, $\tau \subset \partial\kappa$, denotes the (semi)norm associated with the (semi)inner-product

$$(v, w)_\tau = \int_\tau |\mathbf{b}\cdot\mathbf{n}_\kappa| v w\,\mathrm{d}s\,,$$

and c_0 is as defined in (2.5). We remark that the above definition of $|||\cdot|||_{\mathrm{DG}}$ represents a slight modification of the norm considered in [**12**]; in the case $\mathbf{b} \equiv \mathbf{0}$, (3.1) corresponds to the norm proposed by Baumann *et al.* [**4, 19**] and Baker *et al.* [**3**], cf. [**21**].

With this notation, we now provide the following coercivity result for the bilinear form $B_{\mathrm{DG}}(\cdot,\cdot)$ over $S^{\mathbf{p}}(\Omega, \mathcal{T}_h, \mathbf{F}) \times S^{\mathbf{p}}(\Omega, \mathcal{T}_h, \mathbf{F})$.

THEOREM 3.1. *With σ defined as in (2.10), there exists a positive constant C, which depends only on the dimension d and the shape–regularity of $\mathcal{T}_h$, such that*

$$B_{\mathrm{DG}}(v,v) \geq C|||v|||_{\mathrm{DG}}^2 \quad \forall v \in S^{\mathbf{p}}(\Omega,\mathcal{T}_h,\mathbf{F}), \tag{3.2}$$

provided that the constant C_σ arising in the definition of the discontinuity penalization parameter σ is chosen so that:

$$C_\sigma > \begin{cases} 0 & \text{when } \theta = 1\,, \\ C'_\sigma > 0 & \text{when } \theta = -1\,, \end{cases}$$

where C'_σ is a sufficiently large positive constant (see Remark 3.2 below).

PROOF. This result follows by a simple extension of the stability estimates derived by Prudhomme *et al.* [**21**] in the case when $\mathbf{b} \equiv \mathbf{0}$; see also [**12**] for the proof in the case when $\theta = 1$. □

REMARK 3.2. Theorem 3.1 indicates that while the NIP scheme is coercive over $S^{\mathbf{p}}(\Omega,\mathcal{T}_h,\mathbf{F}) \times S^{\mathbf{p}}(\Omega,\mathcal{T}_h,\mathbf{F})$ for any choice of the constant $C_\sigma > 0$ arising in the definition of the discontinuity–penalization parameter σ, the SIP scheme is only coercive if C_σ is chosen sufficiently large. More precisely, C_σ should be selected to be a positive constant which is greater than $C_{\mathrm{t}}C_{\mathrm{reg}}C_e(1+C_{\mathrm{inv}})$, where C_{t} is the constant arising in the multiplicative trace inequality (4.19), C_{reg} stems from the local regularity assumption $\bar{a}_\kappa p_\kappa^2/h_\kappa \leq C_{\mathrm{reg}}\langle \bar{a}p^2\rangle/\langle h\rangle$ for all faces $e \subset \partial\kappa$ and all $\kappa \in \mathcal{T}_h$, $C_e = \max_{\kappa\in\mathcal{T}_h} \mathrm{card}\,\{e \in \Gamma_{\mathrm{int}} \cup \Gamma_{\mathrm{D}} : e \subset \partial\kappa\}$ and C_{inv} is the constant in the inverse inequality $\|\nabla v\|_{L_2(\kappa)} \leq C_{\mathrm{inv}}(p_\kappa^2/h_\kappa)\|v\|_{L_2(\kappa)}$, where $\kappa \in \mathcal{T}_h$ and $v \in S^{\mathbf{p}}(\Omega,\mathcal{T}_h,\mathbf{F})$, cf. Schwab [**24**]. Since the mesh $\mathcal{T}_h$ is assumed to be shape–regular, C_{t}, C_e, C_{reg} and C_{inv} exist and are independent of the discretization parameters.

For the proceeding error analysis, we assume that the solution u to the boundary value problem (2.1), (2.3) is sufficiently smooth: namely, $u \in H^2(\Omega,\mathcal{T}_h)$ and the functions u and $(a\nabla u)\cdot\mathbf{n}_e$ are continuous across each face $e \subset \partial\kappa\backslash\Gamma$ that intersects the subdomain of ellipticity, $\Omega_a = \{x \in \bar{\Omega} : \boldsymbol{\zeta}^{\mathrm{T}}a(x)\boldsymbol{\zeta} > 0 \ \forall \boldsymbol{\zeta} \in \mathbb{R}^d\}$. If this smoothness requirement is violated, the discretization method has to be modified accordingly, cf. [**12**]. We note that under these assumptions, the following Galerkin orthogonality property holds:

$$B_{\mathrm{DG}}(u-u_{\mathrm{DG}},v) = 0 \quad \forall v \in S^{\mathbf{p}}(\Omega,\mathcal{T}_h,\mathbf{F})\,. \tag{3.3}$$

It will be assumed in the proceeding analysis, as well as in Section 4.2, that the velocity vector $\mathbf{b}$ satisfies the following assumption:

$$\mathbf{b}\cdot\nabla_{\mathcal{T}_h} v \in S^{\mathbf{p}}(\Omega,\mathcal{T},\mathbf{F}) \quad \forall v \in S^{\mathbf{p}}(\Omega,\mathcal{T},\mathbf{F})\,. \tag{3.4}$$

To ensure that (2.1) is then meaningful (*i.e.*, that the characteristic curves of the differential operator $\mathcal{L}$ are correctly defined), we still assume that $\mathbf{b} \in \left[W_\infty^1(\Omega)\right]^d$.

Let us denote by Π_p the orthogonal projector in $L_2(\Omega)$ onto the finite element space $S^{\mathbf{p}}(\Omega,\mathcal{T},\mathbf{F})$; *i.e.*, given that $u \in L_2(\Omega)$, we define $\Pi_p u$ by

$$(u-\Pi_p u, v) = 0 \quad \forall v \in S^{\mathbf{p}}(\Omega,\mathcal{T},\mathbf{F})\,,$$

where $(\cdot,\cdot)$ denotes the $L_2(\Omega)$ inner product. We remark that this choice of projector is essential in the following *a priori* error analysis, in order to ensure that

$$(u-\Pi_p u, \mathbf{b}\cdot\nabla_{\mathcal{T}_h} v) = 0 \tag{3.5}$$

for all v in $S^{\mathbf{p}}(\Omega,\mathcal{T},\mathbf{F})$, cf. the proofs of Lemma 3.3 and Theorem 4.4 below. We remark that if the scheme (2.9) is supplemented by streamline–diffusion stabilization, then a different choice of Π_p may be employed which maximizes its hp–approximation properties, cf. [**11, 26**], for example. In that case hypothesis (3.4) is redundant.

We now decompose the global error $u-u_{\mathrm{DG}}$ as

$$u-u_{\mathrm{DG}}=(u-\Pi_p u)+(\Pi_p u-u_{\mathrm{DG}})\equiv\eta+\xi\,. \tag{3.6}$$

With these definitions we have the following result.

LEMMA 3.3. *Assume that (2.4) and (3.4) hold and let* $\beta_1|_\kappa=\|c/(c_0)^2\|_{L_\infty(\kappa)}$*; then the functions* ξ *and* η *defined by (3.6) satisfy the following inequality*

$$\begin{aligned}|||\xi|||_{\mathrm{DG}}^2 \;\leq\; C\Bigg(&\sum_{\kappa\in\mathcal{T}_h}\Big(\|\sqrt{a}\nabla\eta\|_{L_2(\kappa)}^2+\beta_1^2\|c_0\eta\|_{L_2(\kappa)}^2+\|\eta^+\|_{\partial_+\kappa\cap\Gamma}^2+\|\eta^-\|_{\partial_-\kappa\setminus\Gamma}^2\Big)\\&+\int_{\Gamma_{\mathrm{int}}\cup\Gamma_{\mathrm{D}}}\frac{1}{\sigma}\langle(a\nabla\eta)\cdot\mathbf{n}_e\rangle^2\,\mathrm{d}s+\int_{\Gamma_{\mathrm{int}}\cup\Gamma_{\mathrm{D}}}\sigma[\eta]^2\,\mathrm{d}s\Bigg)\,,\end{aligned}$$

where C *is a positive constant that depends only on the dimension* d *and the shape–regularity of* $\mathcal{T}_h$*.*

PROOF. From the Galerkin orthogonality condition (3.3), we deduce that

$$B_{\mathrm{DG}}(\xi,\xi)=-B_{\mathrm{DG}}(\eta,\xi)\,,$$

where ξ and η are as defined in (3.6). Thereby, employing the coercivity result stated in Theorem 3.1, gives

$$|||\xi|||_{\mathrm{DG}}^2\leq-\frac{1}{C}B_{\mathrm{DG}}(\eta,\xi)\,. \tag{3.7}$$

Using the identity (3.5), the right–hand side of (3.7) may be bounded as follows:

$$\begin{aligned}B_{\mathrm{DG}}(\eta,\xi) \;\leq\; C|||\xi|||\Bigg(&\sum_{\kappa\in\mathcal{T}_h}\Big(\|\sqrt{a}\nabla\eta\|_{L_2(\kappa)}^2+\beta_1^2\|c_0\eta\|_{L_2(\kappa)}^2+\|\eta^+\|_{\partial_+\kappa\cap\Gamma}^2\\&+\|\eta^-\|_{\partial_-\kappa\setminus\Gamma}^2\Big)+\int_{\Gamma_{\mathrm{int}}\cup\Gamma_{\mathrm{D}}}\frac{1}{\sigma}\langle(a\nabla\eta)\cdot\mathbf{n}_e\rangle^2\,\mathrm{d}s+\int_{\Gamma_{\mathrm{int}}\cup\Gamma_{\mathrm{D}}}\sigma[\eta]^2\,\mathrm{d}s\Bigg)^{1/2}\;;\end{aligned} \tag{3.8}$$

see [**27**] for details (cf. also [**12**]). On substituting (3.8) into (3.7) we obtain the desired result. □

In the next section, we consider the *a posteriori* and *a priori* error analysis of the hp–version discontinuous Galerkin finite element method (2.9) in terms of certain linear target functionals of practical interest.

4. *A posteriori* and *a priori* error analysis

Very often in problems of practical importance the quantity of interest is an output or target functional $J(\cdot)$ of the solution. Relevant examples include the lift and drag coefficients for a body immersed into a viscous fluid, the local mean value of the field, or its flux through the outflow boundary of the computational domain. The aim of this section is to develop the *a posteriori* and *a priori* error analysis for general linear target functionals $J(\cdot)$ of the solution; for related work, we refer to [**7, 10, 16, 17, 25**], for example.

4.1. Type I *a posteriori* error analysis. In this section we consider the derivation of so-called Type I (cf. [**16**]) or weighted *a posteriori* error bounds. Following the argument presented in [**16, 25**] we begin our analysis by considering the following *dual* or *adjoint* problem: find $z \in H^2(\Omega, \mathcal{T}_h)$ such that

$$B_{\rm DG}(w, z) = J(w) \quad \forall w \in H^2(\Omega, \mathcal{T}_h). \tag{4.1}$$

Let us assume that (4.1) possesses a unique solution. Clearly, the validity of this assumption depends on the choice of the linear functional under consideration. We shall return to this issue at the end of this section; see also the discussion presented in [**16**].

For a given linear functional $J(\cdot)$ the proceeding *a posteriori* error bound will be expressed in terms of the finite element residual $R_{\rm int}$ defined on $\kappa \in \mathcal{T}_h$ by

$$R_{\rm int}|_\kappa = (f - \mathcal{L}u_{\rm DG})|_\kappa \,,$$

which measures the extent to which $u_{\rm DG}$ fails to satisfy the differential equation on the union of the elements κ in the mesh $\mathcal{T}_h$; thus we refer to $R_{\rm int}$ as the *internal residual*. Also, since $u_{\rm DG}$ only satisfies the boundary conditions approximately, the differences $g_{\rm D} - u_{\rm DG}$ and $g_{\rm N} - (a\nabla u_{\rm DG})\cdot\mathbf{n}$ are not necessarily zero on $\Gamma_{\rm D} \cup \Gamma_-$ and $\Gamma_{\rm N}$, respectively; thus we define the *boundary residuals* $R_{\rm D}$ and $R_{\rm N}$ by

$$\begin{aligned} R_{\rm D}|_{\partial\kappa\cap(\Gamma_{\rm D}\cup\Gamma_-)} &= (g_{\rm D} - u^+_{\rm DG})|_{\partial\kappa\cap(\Gamma_{\rm D}\cup\Gamma_-)} \,, \\ R_{\rm N}|_{\partial\kappa\cap\Gamma_{\rm N}} &= (g_{\rm N} - (a\nabla u^+_{\rm DG})\cdot\mathbf{n})|_{\partial\kappa\cap\Gamma_{\rm N}} \,, \end{aligned}$$

respectively.

With this notation, after application of the divergence theorem, the Galerkin orthogonality condition (3.3) may be written in the following equivalent form:

$$\begin{aligned} B_{\rm DG}(u - u_{\rm DG}, v) &= \ell_{\rm DG}(v) - B_{\rm DG}(u_{\rm DG}, v) \\ &= \sum_{\kappa\in\mathcal{T}_h} \Bigg(\int_\kappa R_{\rm int} v \,{\rm d}x - \int_{\partial_-\kappa\cap\Gamma} (\mathbf{b}\cdot\mathbf{n}_\kappa)\, R_{\rm D} v^+ \,{\rm d}s \\ &\quad + \int_{\partial_-\kappa\setminus\Gamma} (\mathbf{b}\cdot\mathbf{n}_\kappa)\,[u_{\rm DG}] v^+ \,{\rm d}s + \int_{\partial\kappa\cap\Gamma_{\rm D}} \theta\, R_{\rm D}((a\nabla v^+)\cdot\mathbf{n}_\kappa) \,{\rm d}s \\ &\quad + \int_{\partial\kappa\cap\Gamma_{\rm D}} \sigma R_{\rm D} v^+ \,{\rm d}s + \int_{\partial\kappa\cap\Gamma_{\rm N}} R_{\rm N} v^+ \,{\rm d}s \\ &\quad - \int_{\partial\kappa\setminus\Gamma} \left\{ \frac{\theta}{2}\,[u_{\rm DG}](a\nabla v^+)\cdot\mathbf{n}_\kappa + \frac{1}{2}[(a\nabla u_{\rm DG})\cdot\mathbf{n}_\kappa] v^+ \right\} {\rm d}s \\ &\quad - \int_{\partial\kappa\setminus\Gamma} \sigma [u_{\rm DG}] v^+ \,{\rm d}s \Bigg) \\ &= 0 \end{aligned} \tag{4.2}$$

for all $v \in S^{\mathbf{p}}(\Omega, \mathcal{T}_h, \mathbf{F})$. Here, we have again employed the result (2.15). The starting point for the analysis is the following general result.

THEOREM 4.1. *Let u and $u_{\rm DG}$ denote the solutions of (2.1), (2.3) and (2.9), respectively, and suppose that the dual solution z is defined by (4.1). Then, the following error representation formula holds:*

$$J(u) - J(u_{\rm DG}) = \mathcal{E}_\Omega(u_{\rm DG}, h, p, z - z_{h,p}) \equiv \sum_{\kappa\in\mathcal{T}_h} \eta_\kappa \,, \tag{4.3}$$

where

$$\begin{aligned}\eta_\kappa &= \int_\kappa R_{\rm int}(z-z_{h,p})\,{\rm d}x - \int_{\partial_-\kappa\cap\Gamma}(\mathbf{b}\cdot\mathbf{n}_\kappa)\,R_{\rm D}(z-z_{h,p})^+\,{\rm d}s\\ &+\int_{\partial_-\kappa\setminus\Gamma}(\mathbf{b}\cdot\mathbf{n}_\kappa)\,[u_{\rm DG}](z-z_{h,p})^+\,{\rm d}s + \int_{\partial\kappa\cap\Gamma_{\rm D}}\theta\,R_{\rm D}((a\nabla(z-z_{h,p})^+)\cdot\mathbf{n}_\kappa)\,{\rm d}s\\ &+\int_{\partial\kappa\cap\Gamma_{\rm D}}\sigma R_{\rm D}(z-z_{h,p})^+\,{\rm d}s + \int_{\partial\kappa\cap\Gamma_{\rm N}}R_{\rm N}(z-z_{h,p})^+\,{\rm d}s\\ &-\int_{\partial\kappa\setminus\Gamma}\left\{\frac{\theta}{2}\,[u_{\rm DG}](a\nabla(z-z_{h,p})^+)\cdot\mathbf{n}_\kappa+\frac{1}{2}[(a\nabla u_{\rm DG})\cdot\mathbf{n}_\kappa](z-z_{h,p})^+\right\}{\rm d}s\\ &-\int_{\partial\kappa\setminus\Gamma}\sigma[u_{\rm DG}](z-z_{h,p})^+\,{\rm d}s \qquad (4.4)\end{aligned}$$

for all $z_{h,p}\in S^{\mathbf{p}}(\Omega,\mathcal{T}_h,\mathbf{F})$.

Proof. On choosing $w=u-u_{\rm DG}$ in (4.1) and recalling the linearity of $J(\cdot)$ and the Galerkin orthogonality property (4.2), we deduce that

$$\begin{aligned}J(u)-J(u_{\rm DG}) &= J(u-u_{\rm DG}) = B_{\rm DG}(u-u_{\rm DG},z)\\ &= B_{\rm DG}(u-u_{\rm DG},z-z_{h,p})\,, \qquad (4.5)\end{aligned}$$

and hence (4.3). □

Thereby, on application of the triangle inequality, we deduce the following Type I *a posteriori* error bound.

Corollary 4.2. *Under the assumptions of Theorem 4.1, the following Type I* a posteriori *error bound holds:*

$$|J(u)-J(u_{\rm DG})|\le\mathcal{E}_{|\Omega|}(u_{\rm DG},h,p,z-z_{h,p})\equiv\sum_{\kappa\in\mathcal{T}_h}|\eta_\kappa|\,, \qquad (4.6)$$

where η_κ *is defined as in (4.4).*

As discussed in [**10, 25**], the local weighting terms involving the difference between the dual solution z and its projection/interpolant $z_{h,p}$ onto $S^{\mathbf{p}}(\Omega,\mathcal{T}_h,\mathbf{F})$ appearing in the Type I bound (4.6) provide useful information concerning the global transport of the error. Thereby, we refrain from eliminating the weighting terms involving the (unknown) dual solution z and approximate z numerically; this will be discussed in Section 5. However, before developing the *a priori* error analysis, let us first look at the structure of the dual problem defined by (4.1). To this end, let us suppose that the aim of the computation is to approximate the (weighted) mean value of the solution u; *i.e.*, $J(\cdot)\equiv M_\psi(\cdot)$, where

$$M_\psi(w)=\int_\Omega w\psi\,{\rm d}x$$

and $\psi\in L_2(\Omega)$. Performing integration by parts, we find that the dual solution z must satisfy the following mesh–dependent problem: find z such that

$$\mathcal{L}^*z\equiv-\nabla\cdot(a\nabla z)-\mathbf{b}\cdot\nabla z+cz \;=\; \psi \quad\text{in}\quad \kappa\,, \qquad (4.7)$$

subject to the inter–element conditions

$$(\mathbf{b}\cdot\mathbf{n}_\kappa)[z]+(1+\theta)\langle(a\nabla z)\cdot\mathbf{n}_\kappa\rangle+\sigma[z] = 0 \quad \text{on} \quad \partial_+\kappa\backslash\Gamma\,, \tag{4.8a}$$

$$(1+\theta)\langle(a\nabla z)\cdot\mathbf{n}_\kappa\rangle+\sigma[z] = 0 \quad \text{on} \quad \partial_-\kappa\backslash\Gamma\,, \tag{4.8b}$$

$$[z] = 0 \quad \text{on} \quad \partial\kappa\cap\Omega_a\,, \tag{4.8c}$$

and boundary conditions

$$z = 0 \quad \text{on} \quad \partial\kappa\cap(\Gamma_{\rm D}\cup\Gamma_+)\,, \tag{4.9a}$$

$$(\mathbf{b}\cdot\mathbf{n}_\kappa)z+(a\nabla z)\cdot\mathbf{n}_\kappa = 0 \quad \text{on} \quad \partial\kappa\cap\Gamma_{\rm N}\,, \tag{4.9b}$$

$$(1+\theta)(a\nabla z)\cdot\mathbf{n}_\kappa = 0 \quad \text{on} \quad \partial\kappa\cap\Gamma_{\rm D} \tag{4.9c}$$

for all $\kappa\in\mathcal{T}_h$. In the case when $\theta=-1$, the dependence of the dual solution on the mesh $\mathcal{T}_h$ may be removed. Indeed, in this case, using the continuity of the advective flux and the continuity of z in the domain of ellipticity Ω_a, the dual problem (4.7), (4.8) and (4.9) reduces to finding z such that

$$\mathcal{L}^*z\equiv-\nabla\cdot(a\nabla z)-\mathbf{b}\cdot\nabla z+cz = \psi \quad \text{in} \quad \Omega\,, \tag{4.10a}$$

$$z=0 \quad \text{on} \quad \Gamma_{\rm D}\cup\Gamma_+\,, \qquad (\mathbf{b}\cdot\mathbf{n})z+(a\nabla z)\cdot\mathbf{n} = 0 \quad \text{on} \quad \Gamma_{\rm N}\,. \tag{4.10b}$$

Thereby, for $\theta=-1$ the corresponding dual problem is well–posed for this choice of target functional. We remark that since the dual problem formed by transposing the arguments in the bilinear form $B_{\rm DG}(\cdot,\cdot)$ involves the formal adjoint of the partial differential operator $\mathcal{L}$, $B_{\rm DG}(\cdot,\cdot)$ is referred to as being *adjoint consistent*, cf. Arnold *et al.* [**2**]. On the other hand, when $\theta=1$ the bilinear form $B_{\rm DG}(\cdot,\cdot)$ is no longer adjoint consistent; in this case the term involving the diffusive flux in (4.8a), (4.8b) and (4.9c) no longer vanishes, and the boundary conditions enforce that both z and $(a\nabla z)\cdot\mathbf{n}$ should be equal to zero on $\Gamma_{\rm D}$. Furthermore, the inter–element conditions become inconsistent in the sense that while (4.8c) enforces continuity of z in Ω_a, (4.8b) requires that

$$(a\nabla z)|_{\partial\kappa_i\cap e}\cdot\mathbf{n}_\kappa=-(a\nabla z)|_{\partial\kappa_j\cap e}\cdot\mathbf{n}_\kappa$$

for all edges $e\subset\partial\kappa$, where κ_i and κ_j are two neighboring elements with common edge e. In general both conditions cannot be simultaneously satisfied; indeed, in Section 6, we provide numerical evidence that indicates that for a fixed $h>0$, the dual solution stemming from the NIP scheme may be discontinuous between element interfaces. This lack of regularity in the dual solution when $\theta=1$ will lead to a degradation in the convergence rate of the error in the computed functional $J(\cdot)$ as the finite element space $S^{\mathbf{p}}(\Omega,\mathcal{T}_h,\mathbf{F})$ is enriched. In contrast, when the SIP scheme is employed, the dual problem is simply the adjoint problem, subject to appropriate boundary conditions, which depend on the particular functional of interest, cf. above. Thereby, in this case, optimal rates of convergence will be observed provided the data for the primal and dual problems (2.1), (2.3) and (4.10), respectively, are sufficiently smooth. These remarks will be made more precise in the next section where we consider the *a priori* error analysis of the *hp*–DGFEM (2.9)

4.2. *A priori* error bounds. In this section we derive *a priori* error bounds for the SIP and NIP methods introduced in Section 2.2. We shall use the superscripts SIP and NIP to distinguish between the two methods. Thereby, writing $B^{\rm SIP}_{\rm DG}(\cdot,\cdot)\equiv B_{\rm DG}(\cdot,\cdot)$ when $\theta=-1$ and $B^{\rm NIP}_{\rm DG}(\cdot,\cdot)\equiv B_{\rm DG}(\cdot,\cdot)$ when $\theta=1$,

the numerical solutions $u_{\rm DG}^{\rm SIP}$ and $u_{\rm DG}^{\rm NIP}$ satisfy the following problems: find $u_{\rm DG}^{\rm SIP}$ in $S^{\mathbf{p}}(\Omega,\mathcal{T}_h,\mathbf{F})$ such that

$$B_{\rm DG}^{\rm SIP}(u_{\rm DG}^{\rm SIP},v)=\ell_{\rm DG}(v)\qquad\forall v\in S^{\mathbf{p}}(\Omega,\mathcal{T}_h,\mathbf{F})\,;$$

and find $u_{\rm DG}^{\rm NIP}$ in $S^{\mathbf{p}}(\Omega,\mathcal{T}_h,\mathbf{F})$ such that

$$B_{\rm DG}^{\rm NIP}(u_{\rm DG}^{\rm NIP},v)=\ell_{\rm DG}(v)\qquad\forall v\in S^{\mathbf{p}}(\Omega,\mathcal{T}_h,\mathbf{F})\,,$$

respectively. The starting point for the *a priori* error analysis is the identity (4.5) in the proof of Theorem 4.1. Again, using the above notation, we recall that

$$J(u)-J(u_{\rm DG}^{\rm SIP})=B_{\rm DG}^{\rm SIP}(u-u_{\rm DG}^{\rm SIP},z^{\rm SIP}-z_{h,p}) \tag{4.11}$$

when the SIP scheme is employed, while for the NIP scheme, we have

$$J(u)-J(u_{\rm DG}^{\rm NIP})=B_{\rm DG}^{\rm NIP}(u-u_{\rm DG}^{\rm NIP},z^{\rm NIP}-z_{h,p}) \tag{4.12}$$

for all $z_{h,p}$ in $S^{\mathbf{p}}(\Omega,\mathcal{T}_h,\mathbf{F})$. Here, $z^{\rm SIP}$ and $z^{\rm NIP}$ are the analytical solutions to the following dual problems: find $z^{\rm SIP}\in H^2(\Omega,\mathcal{T}_h)$ such that

$$B_{\rm DG}^{\rm SIP}(w,z^{\rm SIP})=J(w)\quad\forall w\in H^2(\Omega,\mathcal{T}_h)\,;$$

and find $z^{\rm NIP}\in H^2(\Omega,\mathcal{T}_h)$ such that

$$B_{\rm DG}^{\rm NIP}(w,z^{\rm NIP})=J(w)\quad\forall w\in H^2(\Omega,\mathcal{T}_h)\,, \tag{4.13}$$

respectively.

In the following analysis, it will be helpful to rewrite the representation formula (4.12) for the error in the computed functional when the NIP scheme is employed in terms of $z^{\rm SIP}$ rather than the dual solution $z^{\rm NIP}$ stemming from the NIP scheme. The reason for this is that the error analysis will rely on the regularity of the dual solution. While the regularity of the dual solution $z^{\rm SIP}$ may be easily determined since the underlying boundary value problem for the partial differential equation is the adjoint problem, subject to appropriate data, the Sobolev regularity of the solution to the mesh–dependent dual problem (4.13) is not well understood. Indeed, for a fixed $h>0$, we expect that $z^{\rm NIP}$ will not even be a continuous function, cf. the comments at the end of Section 4.1. We first note that

$$J(u)-J(u_{\rm DG}^{\rm NIP})=B_{\rm DG}^{\rm NIP}(u-u_{\rm DG}^{\rm NIP},z^{\rm SIP}-z_{h,p})-2B_e(z^{\rm SIP},u-u_{\rm DG}^{\rm NIP})$$

for all $z_{h,p}$ in $S^{\mathbf{p}}(\Omega,\mathcal{T}_h,\mathbf{F})$. Thereby, the error in the computed target functional $J(\cdot)$, when either scheme is employed, may be written in the following unified way

$$\begin{aligned}J(u)-J(u_{\rm DG}) &= B_{\rm DG}(u-u_{\rm DG},z^{\rm SIP}-z_{h,p})\\ &\quad -(1+\theta)B_e(z^{\rm SIP},u-u_{\rm DG}^{\rm NIP})\end{aligned} \tag{4.14}$$

for all $z_{h,p}$ in $S^{\mathbf{p}}(\Omega,\mathcal{T}_h,\mathbf{F})$. We remark that the second term on the right–hand side of equation (4.14) is only present when the NIP scheme is employed, *i.e.*, when $\theta=1$. Moreover, we expect this term to be of lower order than the first term in (4.14) and will, thereby, lead to suboptimal rates of convergence as the finite element space $S^{\mathbf{p}}(\Omega,\mathcal{T}_h,\mathbf{F})$ is enriched, when the nonsymmetric interior penalty scheme is employed, cf. Theorem 4.4 below.

Before embarking on the *a priori* error analysis, we first state the following result concerning the approximation properties of the orthogonal projector Π_p in $L_2(\Omega)$ introduced in Section 3; for convenience, here we shall restrict ourselves to 1-irregular, shape–regular meshes consisting of affine equivalent d-parallelepiped elements.

LEMMA 4.3. *Suppose that $\kappa \in \mathcal{T}_h$ is a d–parallelepiped of diameter h_κ and that $u|_\kappa \in H^{k_\kappa}(\kappa)$, $k_\kappa \geq 0$, for $\kappa \in \mathcal{T}_h$. Then, the following approximation results hold*

$$\|u - \Pi_p u\|_{L_2(\kappa)} \leq C \frac{h_\kappa^{s_\kappa}}{p_\kappa^{k_\kappa}} \|u\|_{H^{k_\kappa}(\kappa)} , \quad \|u - \Pi_p u\|_{L_2(\partial\kappa)} \leq C \frac{h_\kappa^{s_\kappa - 1/2}}{p_\kappa^{k_\kappa - 1/2}} \|u\|_{H^{k_\kappa}(\kappa)} ,$$

$$|u - \Pi_p u|_{H^1(\kappa)} \leq C \frac{h_\kappa^{s_\kappa - 1}}{p_\kappa^{k_\kappa - 3/2}} \|u\|_{H^{k_\kappa}(\kappa)} , \quad |u - \Pi_p u|_{H^1(\partial\kappa)} \leq C \frac{h_\kappa^{s_\kappa - 3/2}}{p_\kappa^{k_\kappa - 5/2}} \|u\|_{H^{k_\kappa}(\kappa)} ,$$

where $1 \leq s_\kappa \leq \min(p_\kappa + 1, k_\kappa)$ and C is a constant independent of u, h_κ and p_κ, but dependent on the dimension d and the shape–regularity of $\mathcal{T}_h$.

PROOF. See [**12**] for details; see also [**9**] for sharper results in augmented Sobolev spaces. □

For the rest of this section, let us now assume that the polynomial degree vector $\mathbf{p}$, with $p_\kappa \geq 1$ for each $\kappa \in \mathcal{T}_h$, has *bounded local variation*; *i.e.*, there exists a constant $\rho \geq 1$ such that, for any pair of elements κ and κ' which share a $(d-1)$–dimensional face,

$$\rho^{-1} \leq p_\kappa / p_{\kappa'} \leq \rho \, . \tag{4.15}$$

With this hypothesis, combining the above approximation result with Lemma 3.3, we deduce that

$$|||\xi|||_{\mathrm{DG}}^2 \leq C \sum_{\kappa \in \mathcal{T}_h} \left(\alpha \frac{h_\kappa^{2(s_\kappa - 1)}}{p_\kappa^{2(k_\kappa - 3/2)}} + \beta_2 \frac{h_\kappa^{2s_\kappa}}{p_\kappa^{2k_\kappa}} + \gamma \frac{h_\kappa^{2(s_\kappa - 1/2)}}{p_\kappa^{2(k_\kappa - 1/2)}} \right) \|u\|_{H^{k_\kappa}(\kappa)}^2 , \tag{4.16}$$

where $\alpha|_\kappa = \bar{a}_{\tilde{\kappa}}$, $\beta_2|_\kappa = (\beta_1|_\kappa)^2 \, \|c_0\|_{L_\infty(\kappa)}^2$, $(\beta_1|_\kappa = \|c/(c_0)^2\|_{L_\infty(\kappa)}$, cf. Lemma 3.3), $\gamma|_\kappa = \|\mathbf{b}\|_{L_\infty(\kappa)}$ and C is a positive constant that depends only on d, the parameter ρ in (4.15) and the shape–regularity of $\mathcal{T}_h$.

With these approximation results, we now proceed to prove the main result of this section.

THEOREM 4.4. *Let $\Omega \subset \mathbb{R}^d$ be a bounded polyhedral domain, $\mathcal{T}_h = \{\kappa\}$ a shape–regular subdivision of Ω into d–parallelepipeds and $\mathbf{p}$ a polynomial degree vector of bounded local variation. Then, assuming that conditions (2.4), (2.8), and (3.4) on the data hold, and $u|_\kappa \in H^{k_\kappa}(\kappa)$, $k_\kappa \geq 2$, for $\kappa \in \mathcal{T}_h$, $z^{\mathrm{SIP}}|_\kappa \in H^{l_\kappa}(\kappa)$, $l_\kappa \geq 2$, for $\kappa \in \mathcal{T}_h$, the solution $u_{\mathrm{DG}} \in S^{\mathbf{p}}(\Omega, \mathcal{T}_h, \mathbf{F})$ of (2.9) obeys the error bound*

$$\begin{aligned}
&|J(u) - J(u_{\mathrm{DG}})|^2 \\
&\leq C \sum_{\kappa \in \mathcal{T}_h} \left(\alpha \frac{h_\kappa^{2(s_\kappa - 1)}}{p_\kappa^{2(k_\kappa - 3/2)}} + \beta_3 \frac{h_\kappa^{2s_\kappa}}{p_\kappa^{2k_\kappa}} + \gamma \frac{h_\kappa^{2(s_\kappa - 1/2)}}{p_\kappa^{2(k_\kappa - 1/2)}} \right) \|u\|_{H^{k_\kappa}(\kappa)}^2 \\
&\times \left(\sum_{\kappa \in \mathcal{T}_h} \left(\alpha \frac{h_\kappa^{2(t_\kappa - 1)}}{p_\kappa^{2(l_\kappa - 3/2)}} + \beta_4 \frac{h_\kappa^{2t_\kappa}}{p_\kappa^{2l_\kappa}} + \gamma \frac{h_\kappa^{2(t_\kappa - 1/2)}}{p_\kappa^{2(l_\kappa - 1)}} \right) \|z^{\mathrm{SIP}}\|_{H^{l_\kappa}(\kappa)}^2 + (1 + \theta) \, \|z^{\mathrm{SIP}}\|_{2, \mathcal{T}_h}^2 \right)
\end{aligned}$$

for $1 \leq s_\kappa \leq \min(p_\kappa + 1, k_\kappa)$, $1 \leq t_\kappa \leq \min(p_\kappa + 1, l_\kappa)$, $p_\kappa \geq 1$, $\kappa \in \mathcal{T}_h$, where $\alpha|_\kappa = \bar{a}_{\tilde{\kappa}}$, $\beta_3|_\kappa = (1 + (\beta_1|_\kappa)^2) \|c_0\|_{L_\infty(\kappa)}^2$, $(\beta_1|_\kappa = \|c(x)/(c_0(x))^2\|_{L_\infty(\kappa)})$, $\beta_4|_\kappa = \|(c + \nabla \cdot \mathbf{b})/c_0\|_{L_\infty(\kappa)}^2$, $\gamma|_\kappa = \|\mathbf{b}\|_{L_\infty(\kappa)}$ and C is a constant depending on the dimension d, the parameter ρ from (4.15) and the shape–regularity of $\mathcal{T}_h$.

PROOF. Decomposing the error $u - u_{\rm DG}$ as in (3.6), we note from equation (4.14) above that the error in the target functional $J(\cdot)$ may be expressed as follows:

$$\begin{aligned} J(u) - J(u_{\rm DG}) &= B_{\rm DG}(\eta, z^{\rm SIP} - z_{h,p}) + B_{\rm DG}(\xi, z^{\rm SIP} - z_{h,p}) \\ &\quad -(1+\theta)B_e(z^{\rm SIP}, \eta) - (1+\theta)B_e(z^{\rm SIP}, \xi) \\ &\equiv \mathrm{I} + \mathrm{II} + \mathrm{III} + \mathrm{IV}. \end{aligned}$$

Let us first deal with term I. To this end, we define $z_{h,p} = \Pi_p z^{\rm SIP}$; thereby, employing the approximation results stated in Lemma 4.3, after a lengthy, but straightforward calculation, we deduce that

$$\begin{aligned} (\mathrm{I})^2 &\leq C \sum_{\kappa\in\mathcal{T}_h} \left(\alpha \frac{h_\kappa^{2(s_\kappa-1)}}{p_\kappa^{2(k_\kappa-3/2)}} + \|c_0\|^2_{L_\infty(\kappa)} \frac{h_\kappa^{2s_\kappa}}{p_\kappa^{2k_\kappa}} + \gamma \frac{h_\kappa^{2(s_\kappa-1/2)}}{p_\kappa^{2(k_\kappa-1/2)}} \right) \|u\|^2_{H^{k_\kappa}(\kappa)} \\ &\quad \times \sum_{\kappa\in\mathcal{T}_h} \left(\alpha \frac{h_\kappa^{2(t_\kappa-1)}}{p_\kappa^{2(l_\kappa-3/2)}} + \beta_4 \frac{h_\kappa^{2t_\kappa}}{p_\kappa^{2l_\kappa}} + \gamma \frac{h_\kappa^{2(t_\kappa-1/2)}}{p_\kappa^{2(l_\kappa-1)}} \right) \|z^{\rm SIP}\|^2_{H^{l_\kappa}(\kappa)} . \end{aligned} \tag{4.17}$$

Let us now consider Term II. Here, we note that a bound analogous to (3.8) in the proof of Lemma 3.3 holds with η and ξ replaced by ξ and $z^{\rm SIP} - z_{h,p}$ in (3.8), respectively. Indeed, after application of Lemma 4.3, in this case we have

$$\begin{aligned} (\mathrm{II})^2 &\leq C|||\xi|||^2_{\rm DG} \\ &\quad \times \sum_{\kappa\in\mathcal{T}_h} \left(\alpha \frac{h_\kappa^{2(t_\kappa-1)}}{p_\kappa^{2(l_\kappa-3/2)}} + \beta_4 \frac{h_\kappa^{2t_\kappa}}{p_\kappa^{2l_\kappa}} + \gamma \frac{h_\kappa^{2(t_\kappa-1/2)}}{p_\kappa^{2(l_\kappa-1/2)}} \right) \|z^{\rm SIP}\|^2_{H^{l_\kappa}(\kappa)} . \end{aligned} \tag{4.18}$$

Here we note the importance of selecting $z_{h,p}$ to be the orthogonal projection of $z^{\rm SIP}$ in $L_2(\Omega)$ onto the finite element space $S^{\mathbf{p}}(\Omega, \mathcal{T}_h, \mathbf{F})$, since the identity (3.5) was needed in order to derive (4.18).

In order to bound Terms III and IV, we first note that given an edge $e \subset \partial\kappa$, for some $\kappa \in \mathcal{T}_h$, using the multiplicative trace inequality

$$\|z^{\rm SIP}\|^2_{L_2(e)} \leq C_{\rm t} \left(\|z^{\rm SIP}\|_{L_2(\kappa)} \|\nabla z^{\rm SIP}\|_{L_2(\kappa)} + h_\kappa^{-1} \|z^{\rm SIP}\|^2_{L_2(\kappa)} \right) , \tag{4.19}$$

we deduce that

$$|z^{\rm SIP}|^2_{H^1(e)} \leq \frac{C}{h_\kappa} \|z^{\rm SIP}\|^2_{H^2(\kappa)} .$$

Thereby, employing Lemma 4.3, gives

$$\mathrm{III} \leq C \left(\sum_{\kappa\in\mathcal{T}_h} \alpha \frac{h_\kappa^{2(s_\kappa-1)}}{p_\kappa^{2(k_\kappa-1/2)}} \|u\|^2_{H^{k_\kappa}(\kappa)} \right)^{1/2} \|z^{\rm SIP}\|_{2,\mathcal{T}_h} , \tag{4.20}$$

$$\mathrm{IV} \leq C|||\xi|||_{\rm DG} \|z^{\rm SIP}\|_{2,\mathcal{T}_h} . \tag{4.21}$$

Finally, collecting the bounds on terms I, II, III and IV given in (4.17), (4.18), (4.20) and (4.21), respectively, and employing (4.16) gives the statement of the theorem. □

Let us now discuss some special cases of the general error bound derived in Theorem 4.4. For simplicity, we assume uniform orders $p_\kappa = p$, $s_\kappa = s$, $t_\kappa = t$, $k_\kappa = k$, $l_\kappa = l$, s, t, k and l integers, and $h_\kappa = h$ for all κ in $\mathcal{T}_h$. In the diffusion–dominated case, Theorem 4.4 indicates that the error in the computed functional

may be bounded as follows

$$|J(u) - J(u_{\mathrm{DG}})| \leq C\,\frac{h^{s+t-2}}{p^{k+l-2}}\,p\,\|u\|_{H^k(\Omega)}\|z^{\mathrm{SIP}}\|_{H^l(\Omega)} + (1+\theta)\,\frac{h^{s-1}}{p^{k-3/2}}\,\|u\|_{H^k(\Omega)}\|z^{\mathrm{SIP}}\|_{H^2(\Omega)}\,, \tag{4.22}$$

where $1 \leq s \leq \min(p+1,k)$ and $1 \leq t \leq \min(p+1,l)$. Thereby, when the SIP scheme is employed, *i.e.*, when $\theta = -1$, this error bound is optimal with respect to h and suboptimal in p by a full order. However, when $\theta = 1$, this error bound indicates that the error in the computed target functional behaves like $\mathcal{O}(h^{s-1}/p^{s-3/2})$ as $h \to 0$ and $p \to \infty$. Therefore the 'order–doubling' of the rate of convergence in $|J(u) - J(u_{\mathrm{DG}})|$ observed when the SIP scheme is employed is lost when the NIP method is implemented; this will be numerically verified in Section 6. Finally, we note that in the strictly hyperbolic case ($a \equiv 0$), the error bound in Theorem 4.4 becomes

$$|J(u) - J(u_{\mathrm{DG}})| \leq C\,\frac{h^{s+t-1}}{p^{k+l-1}}\,p^{1/2}\,\|u\|_{H^k(\Omega)}\|z^{\mathrm{SIP}}\|_{H^l(\Omega)}\,.$$

This bound is optimal in h and suboptimal in p by $p^{1/2}$; this is analogous to the bound derived in [**16**], though the proof presented in [**16**] was based on a completely different argument.

5. Adaptive algorithm

For a user-defined tolerance TOL, we now consider the problem of designing an hp–finite element space $S^{\mathbf{p}}(\Omega, \mathcal{T}_h, \mathbf{F})$ such that

$$|J(u) - J(u_{\mathrm{DG}})| \leq \mathtt{TOL}\,, \tag{5.1}$$

subject to the constraint that the total number of degrees of freedom in $S^{\mathbf{p}}(\Omega, \mathcal{T}_h, \mathbf{F})$ is minimized. Following the discussion presented [**16**], we exploit the *a posteriori* error bound (4.6) with z replaced by a discontinuous Galerkin approximation $\hat{z}$ computed on the same mesh $\mathcal{T}_h$ used for the primal solution u_{DG}, but with a higher degree polynomial, *i.e.*, $\hat{z} \in S^{\hat{\mathbf{p}}}(\Omega, \mathcal{T}_h, \mathbf{F})$, $\hat{\mathbf{p}} = \mathbf{p} + \mathbf{p}_{\mathrm{inc}}$; in Section 6, we set $\mathbf{p}_{\mathrm{inc}} = \mathbf{1}$, cf. [**10, 14, 25**]. Thereby, in practice we enforce the stopping criterion

$$\hat{\mathcal{E}}_{|\Omega|} \equiv \mathcal{E}_{|\Omega|}(u_{\mathrm{DG}}, h, p, \hat{z} - z_{h,p}) \leq \mathtt{TOL}\,. \tag{5.2}$$

If (5.2) is not satisfied, then the elements are marked for refinement/derefinement according to the size of the (approximate) error indicators $|\hat{\eta}_\kappa|$; these are defined analogously to $|\eta_\kappa|$ in (4.4) with z replaced by $\hat{z}$. In Section 6, we use the fixed fraction mesh refinement algorithm, with refinement and derefinement fractions set to 20% and 10%, respectively.

Once an element $\kappa \in \mathcal{T}_h$ has been flagged for refinement or derefinement, a decision must be made whether the local mesh size h_κ or the local degree p_κ of the approximating polynomial should be adjusted accordingly. The choice to perform either h–refinement/derefinement or p–refinement/derefinement is based on the local smoothness of the primal and dual solutions u and z, respectively; cf. [**14, 16**]. Let us first consider the case when an element has been flagged for refinement. If u or z are locally smooth, then p–refinement will be more effective than h–refinement, since the error will be expected to decay quickly within the current element κ as p_κ is increased. On the other hand, if both u and z have low regularity within the

element κ, then h–refinement will be performed. To ensure that the desired level of accuracy is achieved efficiently, in [**16**] an automatic procedure was developed for deciding when to h– or p–refine, based on the smoothness–estimation strategy proposed by Ainsworth & Senior [**1**]. For a review of various hp–adaptive strategies as well as a description of a new algorithm based on Sobolev index estimation *via* local Legendre expansions, we refer to [**14**].

If an element has been flagged for derefinement, then the strategy implemented here is to coarsen the mesh in low–error–regions where either the primal or dual solutions u and z, respectively, are smooth and decrease the degree of the approximating polynomial in low–error–regions when both u and z are insufficiently regular, cf. [**16**].

6. Numerical experiments

In this section we present a number of experiments to numerically verify the *a priori* error bound derived in Section 4.2, as well as to demonstrate the performance of the hp–adaptive algorithm outlined in Section 5.

6.1. Example 1. In this first example, we investigate the performance of the symmetric ($\theta = -1$) and nonsymmetric ($\theta = 1$) versions of the interior penalty method (cf. (2.9)) for the discretization of a second–order uniformly elliptic partial differential equation. We consider Poisson's equation on the unit square $\Omega = (0,1)^2$, where $a = I$, $\mathbf{b} \equiv \mathbf{0}$, $c \equiv 0$, and f is selected so that the analytical solution to (2.1) is given by

$$u(x,y) = \frac{(1+x)^2}{4}\,\sin(2\pi xy)\,.$$

Furthermore, we choose the functional of interest $J(\cdot)$ to represent the (weighted) mean value of u over Ω, *i.e.*,

$$J(u) \equiv M_\psi(u) = \int_\Omega u\psi\,\mathrm{d}x\,;$$

here, we define the weight function ψ by

$$\psi = \sin^2(2\pi x)\sin^2(2\pi y)\mathrm{e}^{-(x+y)}\,.$$

Thereby, the true value of the functional is given by $J(u) = 0.02438990598636878$.

In Figure 1 we present a comparison of the error in the functional $|J(u) - J(u_{\mathrm{DG}})|$ with the mesh size h for $p = 1,2,3,4$, employing the SIP method with $C_\sigma = 10$. Here, we observe that $|J(u) - J(u_{\mathrm{DG}})|$ converges to zero at the (optimal) rate $\mathcal{O}(h^{2p})$ as the mesh is refined for each fixed p, cf. Theorem 4.4. In contrast, Figure 2 indicates that $|J(u)-J(u_{\mathrm{DG}})|$ behaves like $\mathcal{O}(h^{p+1})$ for odd p and like $\mathcal{O}(h^p)$ for even p when the NIP method is employed with $C_\sigma = 10$. The sub-optimal convergence observed in the latter (nonsymmetric) scheme is attributed to the lack of smoothness in the resulting dual problem, cf. the remarks made at the end of Section 4.1. As noted in Section 4, the dual problem arising from the symmetric version of the DGFEM involves the adjoint partial differential operator supplemented with appropriate data depending on the choice of the target functional of interest. In our case the dual problem is as follows: find z such that

$$-\Delta z = \psi \;\text{ in }\; \Omega,\; z = 0 \;\text{ on }\; \partial\Omega.$$

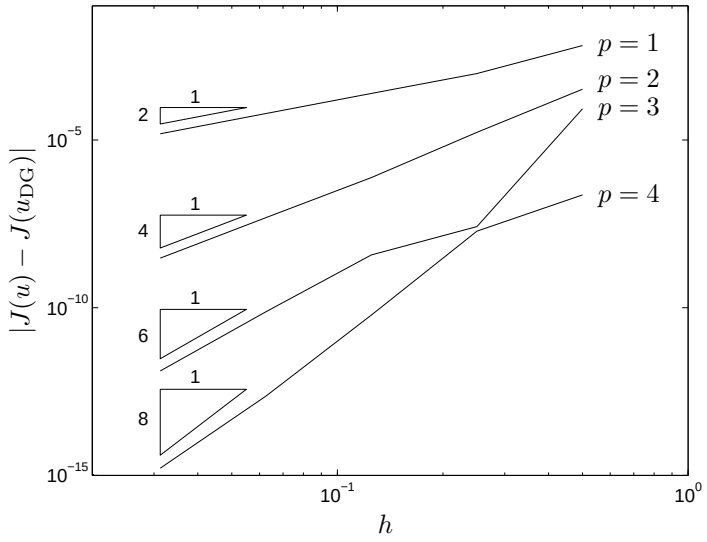

FIGURE 1. Example 1. Convergence of the symmetric interior penalty DGFEM with h–refinement.

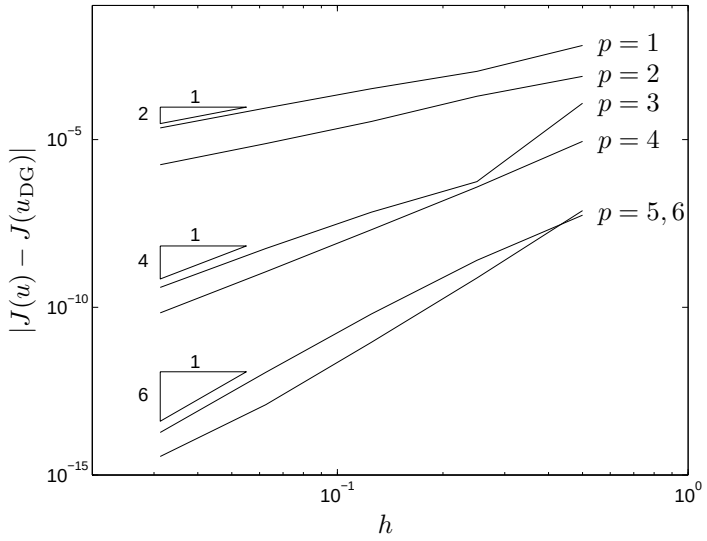

FIGURE 2. Example 1. Convergence of the nonsymmetric interior penalty DGFEM with h–refinement.

Given that ψ is an analytic function in $\bar{\Omega}$, z will also be analytic in any closed subdomain of $\bar{\Omega}$ which excludes the four corners.

In contrast, Section 4.1 indicates that the NIP method gives rise to a mesh dependent dual problem whose analytical solution will in general not be continuous. Indeed, in Figure 3 we plot the profile of the numerical approximation of the dual solution along $y = 0.28$, $0 \leq x \leq 1$, computed using both the symmetric and nonsymmetric versions of the DGFEM on a uniform 5×5 square mesh with $\hat{\mathbf{p}} = \mathbf{4}$.

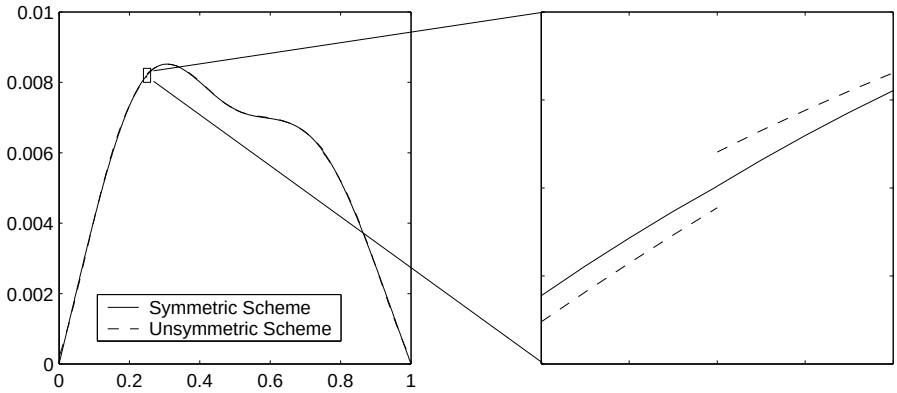

FIGURE 3. Example 1. Profile of the dual solution along $y = 0.28$, $0 \leq x \leq 1$, computed using both the symmetric and nonsymmetric version of the interior penalty method on a uniform 5×5 square mesh with $\hat{\mathbf{p}} = \mathbf{4}$.

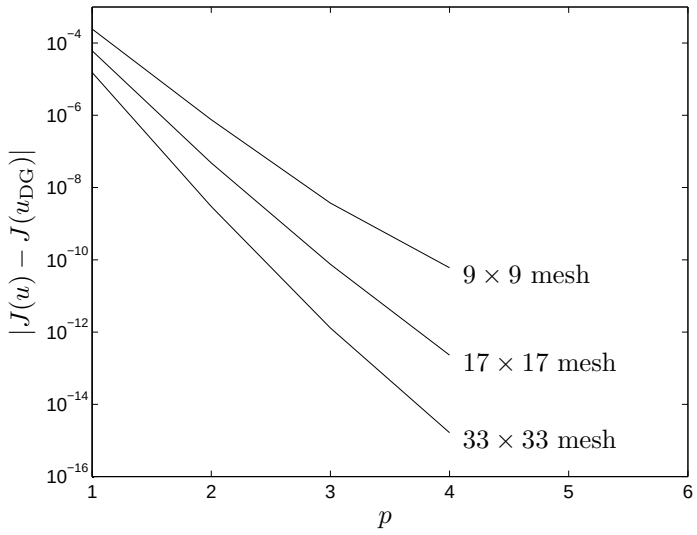

FIGURE 4. Example 1. Convergence of the symmetric interior penalty DGFEM with p–refinement.

Here, we clearly see that while the dual solution computed using the symmetric scheme is essentially continuous, the dual solution arising from the nonsymmetric scheme is discontinuous between element interfaces. We note that the 'jumps' in the latter dual solution present at inter-element boundaries persist even as the mesh is enriched. The lack of regularity in z leads to the sub-optimal rates of convergence observed in Figure 2 when the nonsymmetric version of the DGFEM is employed.

Finally, in Figures 4 and 5, respectively, we investigate the convergence of the symmetric and nonsymmetric versions of the DGFEM with p–enrichment for fixed

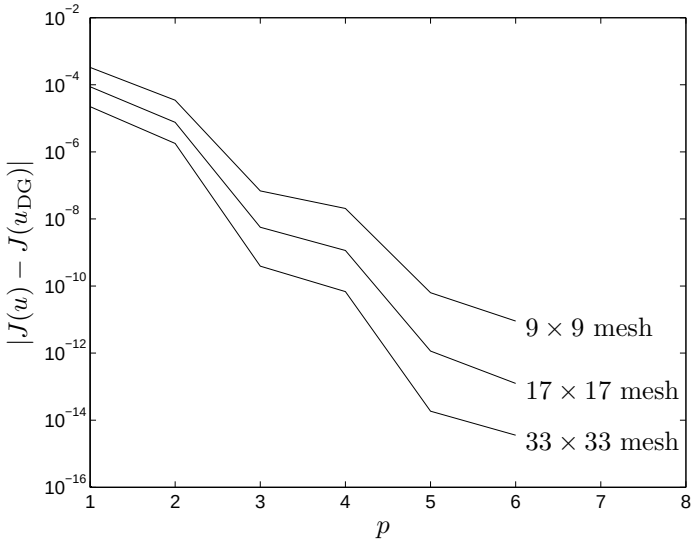

FIGURE 5. Example 1. Convergence of the nonsymmetric interior penalty DGFEM with p–refinement.

h. Since the primal solution u is a (real) analytic function, we expect to observe an exponential rate of convergence under p-refinement. Indeed, Figures 4 and 5 clearly illustrate this behavior: on a linear–log scale, the convergence plots for each h become (on average) straight lines as the degree of the approximating polynomial is increased. This is true for both the SIP and the NIP scheme. We remark that the convergence lines in Figure 4 are steeper than those in Figure 5, since the dual solution corresponding to the symmetric IP-DGFEM is also smooth, while z is not even continuous when the nonsymmetric scheme is employed.

6.2. Example 2. In this second example we investigate the performance of the hp–adaptive strategy outlined in Section 5 for the (symmetric) version of the interior penalty method applied to a mixed hyperbolic–elliptic problem with discontinuous boundary data. We let $a = \varepsilon(x)I$, where

$$\varepsilon = \frac{\delta}{2}(1 - \tanh((r - 1/4)(r + 1/4)/\gamma))\,,$$

$r^2 = (x - 1/2)^2 + (y - 1/2)^2$ and $\delta \geq 0$ and $\gamma > 0$ are constants. Suppose, furthermore, that $\mathbf{b} = (2y^2 - 4x + 1, 1 + y)$, $c = -\nabla \cdot \mathbf{b}$ and $f = 0$.

The characteristics associated with the hyperbolic part of the operator enter the computational domain Ω from three sides of Γ, namely through the vertical edges placed along $x = 0$ and $x = 1$ and the horizontal edge along $y = 0$; the characteristics exit Ω through the horizontal edge along $y = 1$. Thus, on the inflow part of Γ we prescribe the following boundary condition:

$$u(x,y) = \begin{cases} 1 & \text{for } x = 0\ ,\ 0 < y \leq 1\,, \\ \sin^2(\pi x) & \text{for } 0 \leq x \leq 1\ ,\ y = 0\,, \\ \mathrm{e}^{-50y^4} & \text{for } x = 1\,,\ 0 < y \leq 1\,. \end{cases}$$

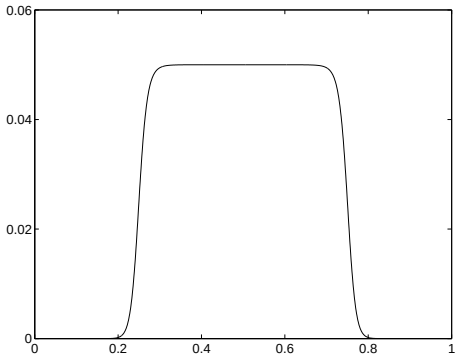

FIGURE 6. Example 2. Profile of ε along $y = 0.5$, $0 \leq x \leq 1$.

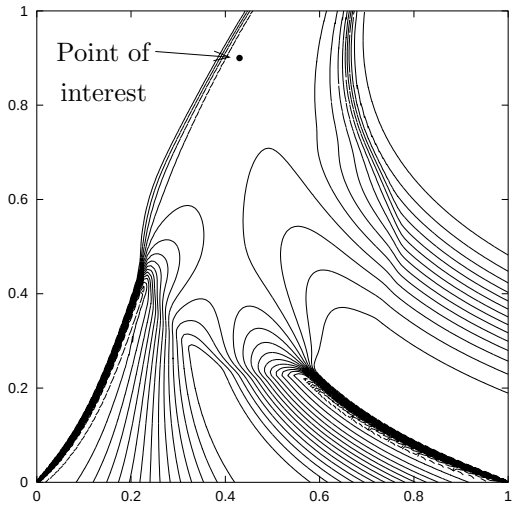

FIGURE 7. Example 2. DGFEM approximation to the primal problem on a 129×129 mesh with piecewise bilinear elements ($\mathbf{p} = \mathbf{1}$).

This is a variant of the test problem presented in [**15**]. We note that, with $\delta > 0$ and $0 < \gamma \ll 1$, the diffusion parameter ε will be approximately equal to δ in the circular region defined by $r < 1/4$, where the underlying partial differential equation is uniformly elliptic. In this example, we set $\delta = 0.05$ and $\gamma = 0.01$; a cross section of ε along $0 \leq x \leq 1$, $y = 1/2$ is shown in Figure 6. As r is increased beyond $1/4$, ε rapidly decreases through a layer of width $\mathcal{O}(\gamma)$; for example, when $r > 0.336$ we have $\varepsilon < 10^{-15}$, so from the computational point of view ε is zero to within rounding error; in this region, the partial differential equation undergoes a change of type becoming, in effect, hyperbolic. Thus we shall refer to the part of Ω with $r > 1/4 + \mathcal{O}(\gamma)$ as the *hyperbolic region*, while the set of points in Ω with $r \leq 1/4$ will be called the *elliptic region*. [Of course, strictly speaking, the partial differential equation is elliptic in the whole of $\bar{\Omega}$.] Furthermore, Figure 7 depicts the

TABLE 1. Example 2: Adaptive algorithm using h–refinement

Nodes	Elements	DOF	$\lvert J(u) - J(u_{\mathrm{DG}})\rvert$	$\sum_\kappa \lvert\hat{\eta}_\kappa\rvert$	θ
81	64	256	7.645e-02	6.597e-02	0.86
119	94	376	2.554e-02	6.331e-02	2.48
206	169	676	9.897e-04	5.640e-02	56.99
357	295	1180	1.323e-03	2.180e-02	16.48
638	538	2152	5.743e-04	8.900e-03	15.50
1053	898	3592	4.959e-04	3.936e-03	7.94
1728	1525	6100	1.453e-04	1.678e-03	11.55
2883	2548	10192	9.295e-05	8.622e-04	9.28
4848	4390	17560	6.002e-05	4.232e-04	7.05
8049	7309	29236	3.323e-05	2.234e-04	6.72
13048	11947	47788	1.562e-05	1.192e-04	7.63

numerical approximation to (2.1) using the symmetric Interior Penalty DGFEM on a uniform 129×129 uniform square mesh with $\mathbf{p} = \mathbf{1}$.

Here, we suppose that the aim of the computation is to calculate the value of the analytical solution u at the point of interest $x = (0.43, 0.9)$, *i.e.*,

$$J(u) = u(0.43, 0.9);$$

cf. Figure 7. The true value of the functional is given by $J(u) = 0.704611313375$.

We first study the performance of our adaptive strategy with h–refinement only, and $\mathbf{p} = \mathbf{1}$. In Table 1 we show the number of nodes, elements and degrees of freedom (DOF) in $S^{\mathbf{1}}(\Omega, \mathcal{T}_h, \mathbf{F})$, the true error in the functional $|J(u - u_{\mathrm{DG}})|$, the computed *a posteriori* error bound (4.6) and the corresponding effectivity index θ. Here, we see that the quality of the computed Type I *a posteriori* error bound is extremely good. Indeed, even on relativity coarse meshes, the bound is reliable; moreover, the effectivity index θ shows that $\hat{\mathcal{E}}_{|\Omega|}$ overestimates the true error in the computed functional by a consistent factor as the finite element space $S^{\mathbf{1}}(\Omega, \mathcal{T}_h, \mathbf{F})$ is enriched.

In Figure 8 we show the mesh generated after 9 adaptive mesh refinement steps. Here, we see that the mesh is largely concentrated in the neighborhood upstream of the point of interest, together with some almost uniform refinement of the circular region enclosing the part of the computational domain where the underlying partial differential equation is elliptic. We remark that some refinement of the mesh in the region where the discontinuities enter Ω from $(0, 0)$ and $(1, 0)$, as well as the steep layer entering from the right–hand side boundary has also occurred, though these features of the analytical solution still remain largely unresolved.

The design of the mesh is closely related to the structure of the underlying dual solution, since the weighting terms involving the difference between the (approximated) dual solution $\hat{z}^{\mathrm{SIP}}$ and $z_{h,p}$ multiply the computable residual terms involving

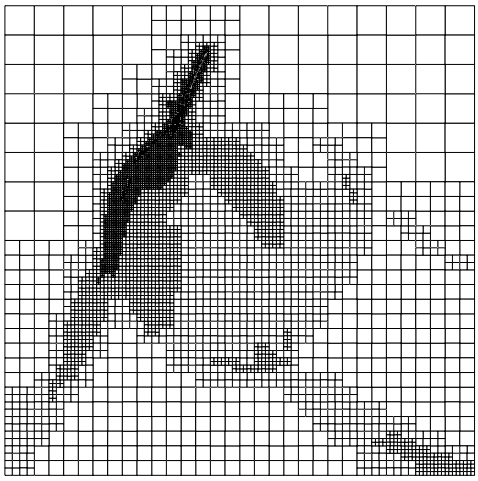

FIGURE 8. Example 2. h–mesh after 9 refinements, with 8049 nodes, 7309 elements and 29236 degrees of freedom; here, $|J(u) - J(u_{\mathrm{DG}})| = 3.323 \times 10^{-5}$.

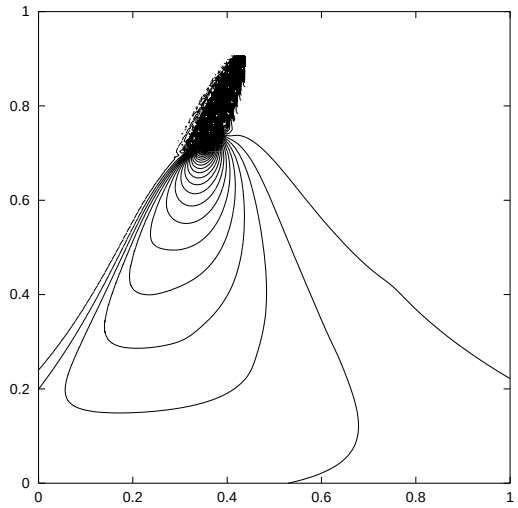

FIGURE 9. Example 2. Dual solution.

the numerical solution u_{DG} in the definition of the local error indicator $|\hat{\eta}_\kappa|$, cf. (4.4) with z^{SIP} replaced by $\hat{z}^{\mathrm{SIP}}$. From Figure 9, we see that in the hyperbolic region of the computational domain above the region of ellipticity, the dual solution consists of a single 'spike' originating from the point of interest which is transported upstream along the single characteristic passing through $x = (0.43, 0.9)$. At the boundary of the circular region where the partial differential equation undergoes a change of type from 'hyperbolic' to elliptic, the spike in the dual solution is 'diffused out'. Consequently, the domain of dependence of the point of interest consists of

TABLE 2. Example 2: Adaptive algorithm using *hp*–refinement

Nodes	Elements	DOF	$\lvert J(u) - J(u_{\mathrm{DG}})\rvert$	$\sum_\kappa \lvert\hat{\eta}_\kappa\rvert$	θ
81	64	576	1.924e-02	3.330e-02	1.73
99	76	740	1.056e-02	1.085e-02	1.03
162	130	1451	1.006e-02	2.290e-02	2.28
241	193	2483	7.400e-04	2.385e-03	3.22
302	244	3776	3.760e-05	2.754e-04	7.32
323	262	4777	1.270e-05	1.026e-04	8.08
396	325	6916	9.896e-06	2.245e-05	2.27
487	403	9941	1.224e-06	6.466e-06	5.28
577	481	13528	4.656e-07	1.163e-06	2.50
713	601	19855	2.449e-07	2.582e-07	1.05
960	820	31019	1.574e-08	3.202e-08	2.03
1313	1132	47406	6.531e-10	2.154e-09	3.30

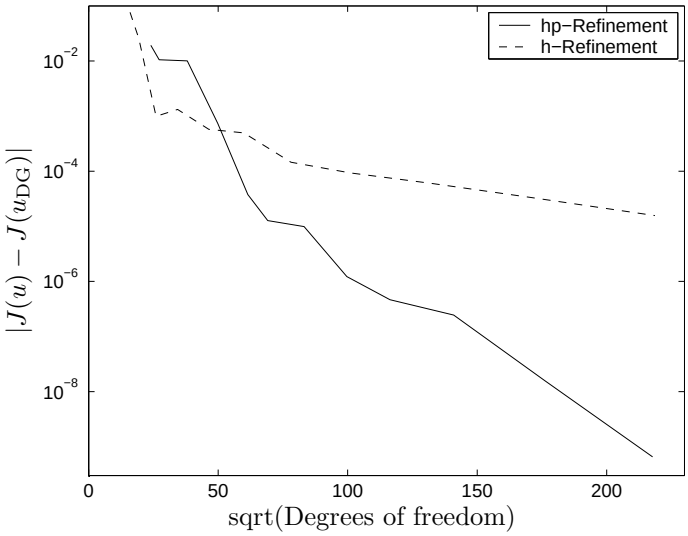

FIGURE 10. Example 2. Comparison between *h*– and *hp*–adaptive mesh refinement

the single characteristic passing through $x = (0.43, 0.9)$, the circular region where the underlying partial differential equation is elliptic, together with the part of the computational domain enclosed by the intersection of the inflow boundary Γ_- and the two extreme characteristics emanating from the circular elliptic region.

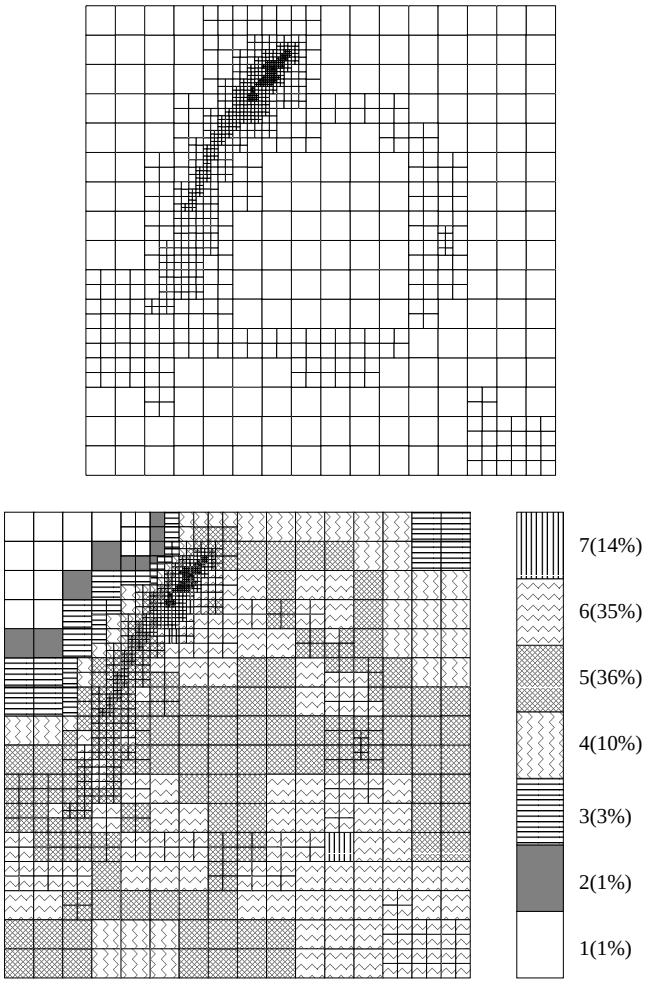

FIGURE 11. Example 2. h– and hp–meshes after 11 refinements, with 1313 nodes, 1132 elements and 47406 degrees of freedom; here, $|J(u) - J(u_{\mathrm{DG}})| = 6.531 \times 10^{-10}$.

Let us now turn our attention to hp–adaptivity; in Table 2 we show the performance of the proposed adaptive finite element algorithm employing hp–refinement. Here, we again see that the quality of the computed Type I *a posteriori* error bound (4.6) is extremely good in the sense that it overestimates the true error in the computed functional by a factor of about 1–8.

In Figure 10 we plot $|J(u) - J(u_{\mathrm{DG}})|$, using both h– and hp–refinement against the square–root of the number of degrees of freedom on a linear–log scale. We see that after the initial transient, the error in the computed functional using hp–refinement becomes (on average) a straight line, thereby indicating exponential convergence of $J(u_{\mathrm{DG}})$ to $J(u)$; this occurs since z^{SIP} is a real analytic function in the regions of the computational domain where u is not smooth and vice versa. Figure 10 also demonstrates the superiority of the adaptive hp–refinement strategy

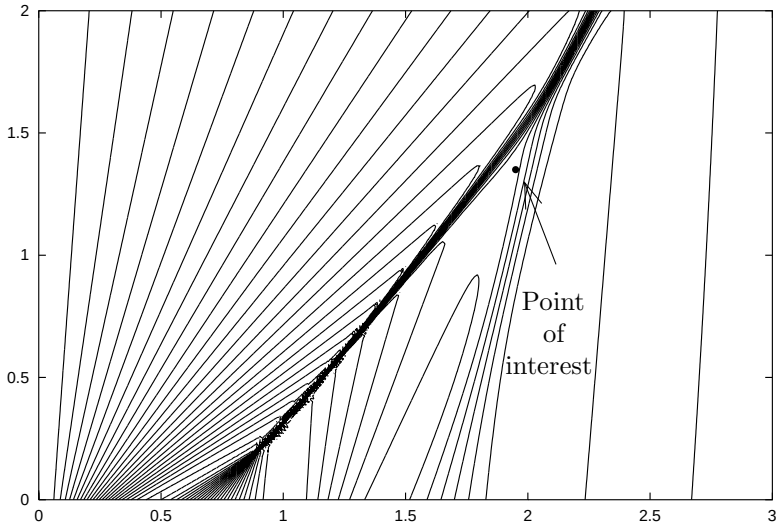

FIGURE 12. Example 3. DGFEM approximation to the primal problem on a 257×171 mesh with piecewise bilinear elements ($\mathbf{p} = \mathbf{1}$).

over the standard adaptive h–refinement algorithm. On the final mesh the true error between $J(u)$ and $J(u_{\mathrm{DG}})$ using hp–refinement is over 4 orders of magnitude smaller than the corresponding quantity when h–refinement is employed alone.

Figure 11 depicts the primal mesh after 11 adaptive mesh refinement steps. For clarity, we show the h–mesh alone, as well as the corresponding distribution of the polynomial degree on this mesh and the percentage of elements with that degree. We see that some h–refinement of the primal mesh has occurred in the region of the computational domain upstream of the point of interest, as well as in the circular region where the underlying partial differential equation changes type. Once the h–mesh has adequately captured the structure of the primal and dual solutions, the hp–adaptive algorithm performs p–refinement elsewhere in the domain of dependence of the point of interest.

6.3. Example 3. In this final example we consider the performance of our hp–adaptive algorithm for the (symmetric) version of the interior penalty method applied to a nonlinear problem; the extension of the above Type I *a posteriori* error analysis to the case of a nonlinear convection–diffusion problem follows directly from the theory developed in the articles [**10, 14, 17, 25**]. Here, we study the one–dimensional unsteady viscous Burgers' equation; i.e., writing y to denote time, we have

$$u_y + \left(\frac{u^2}{2}\right)_x - (\varepsilon(x)u_x)_x = 0, \tag{6.1}$$

where $\varepsilon(x) = (1+\tanh(x-1.75))/200$. We consider the partial differential equation (6.1) on the (space–time) domain $\Omega = (0,3) \times (0,2)$, subject to the initial condition $u(x,0) = 2/(1+x^3)\,\sin^2(\pi x)$, and boundary conditions $u(0,y) = 0$ and $u_x(3,y) = 0$

TABLE 3. Example 3: Adaptive algorithm using hp–refinement

Nodes	Elements	DOF	$\lvert J(u) - J(u_{\mathrm{DG}})\rvert$	$\sum_\kappa \lvert\hat{\eta}_\kappa\rvert$	θ
117	96	864	1.788e-02	1.689e-01	9.44
184	147	1379	2.557e-02	5.080e-02	1.99
249	204	2181	1.562e-03	8.980e-03	5.75
347	285	3394	3.070e-04	2.517e-03	8.20
439	366	5122	9.063e-05	1.012e-03	11.17
500	414	6754	1.929e-05	2.569e-04	13.32
580	483	9828	8.566e-06	3.901e-05	4.55
700	585	13781	3.823e-06	1.916e-05	5.01
897	756	21108	2.765e-06	8.456e-06	3.06
1122	957	28701	4.921e-07	1.168e-06	2.37
1398	1197	40749	8.619e-08	2.521e-07	2.92
2005	1764	65480	2.038e-08	6.142e-08	3.01

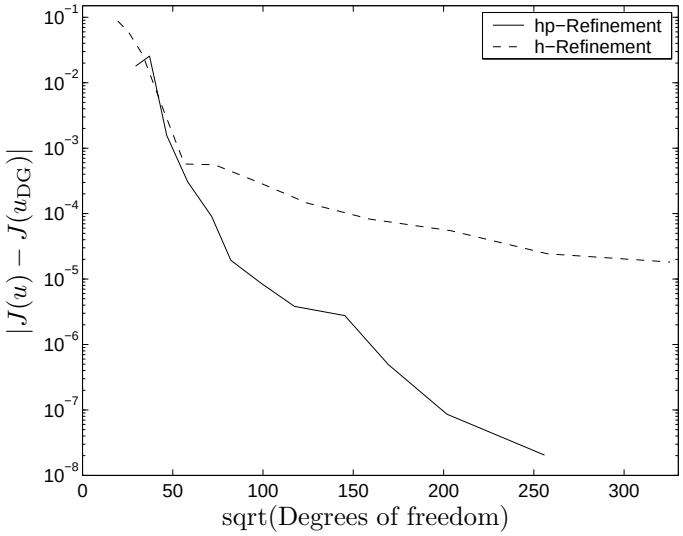

FIGURE 13. Example 3. Comparison between h– and hp–adaptive mesh refinement

for $y \in [0, 2]$. We remark that this is a variant of the inviscid Burgers' example considered in [**10, 13**]. In the inviscid case, the analytical solution to this problem consists of three smooth 'hills' which form shock waves as time increases; these shocks eventually merge to form a single line of discontinuity in the (x, y)–plane.

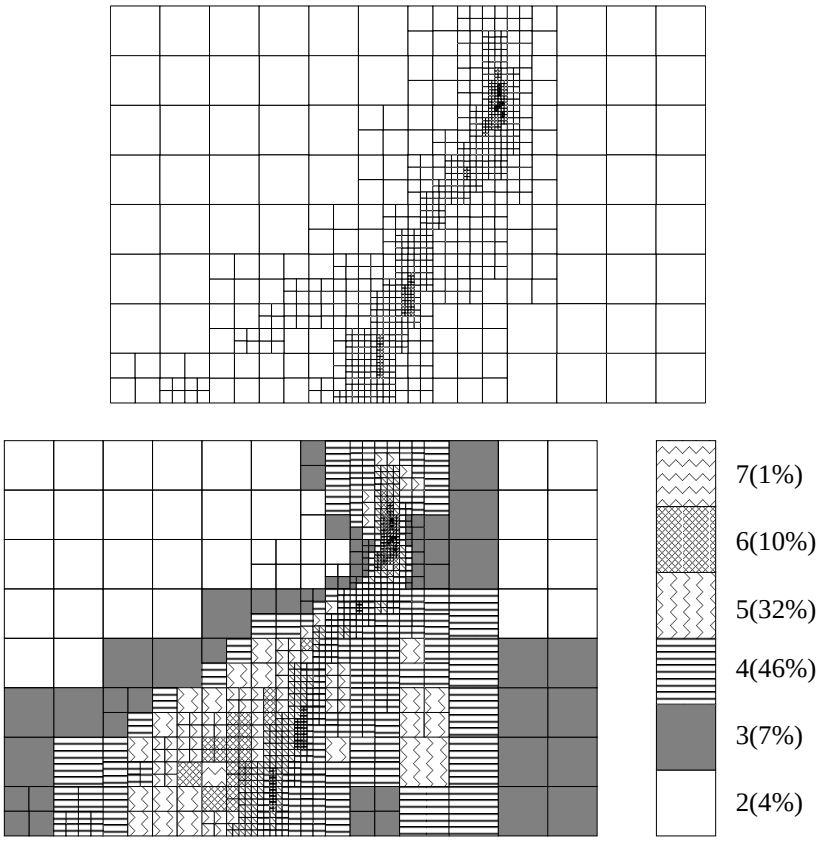

FIGURE 14. Example 3. h– and hp–meshes after 9 refinements, with 1122 nodes, 957 elements and 28701 degrees of freedom; here, $|J(u) - J(u_{\mathrm{DG}})| = 4.921 \times 10^{-7}$.

The introduction of the viscosity term, with coefficient $\varepsilon(x)$, leads to the development of viscous internal layers. In this example, $\varepsilon(x)$ increases as x increases; indeed, on the interval $[0, 3]$, ε attains a minimum value of 2.93×10^{-4} at $x = 0$ and a maximum of 9.24×10^{-3} at $x = 3$. Thereby, the viscous layers become increasing smeared as x increases, cf. Figure 12.

Here, we again suppose that the aim of the computation is to calculate the value of the analytical solution u at a given point of interest x_* in the computational domain Ω; in this example, we select $x_* = (1.95, 1.35)$, cf. Figure 12. In this case, the true value of the functional is given by $J(u) = 0.39448860$. Table 3 demonstrates the performance of the hp–adaptive algorithm for the selected target functional of interest. As for the linear problem presented in Section 6.2, we see that the quality of the computed Type I *a posteriori* error bound is extremely good. Indeed, even on relativity coarse meshes, the bound is reliable; moreover, the effectivity index θ shows that $\hat{\mathcal{E}}_{|\Omega|}$ overestimates the true error in the computed functional by a consistent factor as the finite element space $S^{\mathbf{p}}(\Omega, \mathcal{T}_h, \mathbf{F})$ is enriched.

In Figure 13 we compare the performance of the h– and hp–mesh refinement algorithms for this problem. Again, we observe exponential convergence of the

error in the computed functional using hp–refinement; on the linear–log scale, the convergence line becomes (on average) straight. On the final mesh the true error between $J(u)$ and $J(u_{\mathrm{DG}})$ using hp–refinement is over 3 orders of magnitude smaller than the corresponding quantity when h–refinement is employed alone.

Finally, in Figure 14 we show the primal mesh after 9 adaptive hp–mesh refinements. Here, we see that the h–mesh has been refined in the neighborhood of the point of interest x_* as well as in the region upstream of the x_*, thereby isolating the smooth region of u from the two interacting viscous layers; this renders the subsequent p–refinement in this region much more effective.

7. Concluding remarks

In this paper, we have been concerned with the *a priori* and *a posteriori* error analyses of the hp-version Discontinuous Galerkin Finite Element Method (hp–DGFEM) for second–order partial differential equations with nonnegative characteristic form. We have been particularly interested in the approximation of linear output functionals of the analytic solution. It was shown that the symmetric and nonsymmetric interior penalty versions of the hp–DGFEM exhibit completely different convergence rates: while the approximation obtained from the symmetric version exhibits an optimal rate of convergence, the approximation which is computed by means of the nonsymmetric version converges at an inferior rate due to lack of adjoint consistency. We also explored the implementation of the *a posteriori* error bounds into an hp-adaptive mesh refinement algorithm to compute approximations to linear target functionals of practical interest to within a fixed user–defined tolerance. The performance of the resulting hp–refinement strategy was then studied through a series of numerical experiments. In particular, we demonstrated the superiority of using hp–adaptive mesh refinement over the traditional h–refinement method, where the degree of the approximating polynomial is kept fixed at some low value.

References

[1] M. Ainsworth and B. Senior, *An adaptive refinement strategy for hp–finite element computations*. Appl. Numer. Maths. 26:165–178, 1998.

[2] D. Arnold, F. Brezzi, B. Cockburn and D. Marini, *Unified analysis of discontinuous Galerkin methods for elliptic problems*. SIAM J. Numer. Anal. 39(5):1749–1779, 2002.

[3] G.A. Baker, W.N. Jureidini and O.A. Karakashian, *Piecewise solenoidal vector fields and the Stokes problem*. SIAM J. Numer. Anal. 27(6):1466–1485, 1990.

[4] C. Baumann, *An hp–adaptive discontinuous Galerkin FEM for computational fluid dynamics*. Doctoral Dissertation, TICAM, UT Austin, Texas, 1997.

[5] R. Becker and P. Hansbo, *Discontinuous Galerkin methods for convection-diffusion problems with arbitrary Péclet number*. In: P. Neittaanmäki, T. Tiihonen and P. Tarvainen, editors, Numerical Mathematics and Advanced Applications: Proceedings of the 3rd European Conference. World Scientific, pp. 100–109, 2000.

[6] R. Becker, P. Hansbo and M.G. Larson, *Energy norm a posteriori error estimation for discontinuous Galerkin methods*. Chalmers Finite Element Center Preprint 2001-11, Chalmers University of Technology, Sweden, 2001.

[7] R. Becker and R. Rannacher, *Weighted A Posteriori Error Control in FE Methods*, Preprint 1, Interdisziplinäres Zentrum für Wissenschaftliches Rechnen, Universität Heidelberg, Heidelberg, Germany, 1996.

[8] B. Cockburn, G.E. Karniadakis and C.-W. Shu, *The development of discontinuous Galerkin methods*. In: B. Cockburn, G.E. Karniadakis and C.-W. Shu (eds.) Discontinuous Galerkin Finite Element Methods. Lecture Notes in Computational Science and Engineering, **11**. Springer, 2000.

[9] E. H. Georgoulis and E. Süli, *hp-DGFEM on Shape-Irregular Meshes: Reaction-Diffusion Problems*. Numerical Analysis Group Research Report NA-01/09, Oxford University Computing Laboratory, 2001.

[10] R. Hartmann and P. Houston, *Adaptive discontinuous Galerkin finite element methods for nonlinear hyperbolic conservation laws*. SIAM J. Sci. Comp. (to appear).

[11] P. Houston, Ch. Schwab and E. Süli, *Stabilized hp–finite element methods for first–order hyperbolic problems*. SIAM J. Numer. Anal. 37(5):1618–1643, 2000.

[12] P. Houston, Ch. Schwab and E. Süli, *Discontinuous hp–finite element methods for advection–diffusion–reaction problems,* SIAM J. Numer. Anal. 39(6):2133–2163, 2002.

[13] P. Houston, B. Senior and E. Süli, *hp–Discontinuous Galerkin finite element methods for hyperbolic problems: error analysis and adaptivity*. Int. J. Numer. Meth. Fluids (to appear).

[14] P. Houston, B. Senior and E. Süli, *Sobolev regularity estimation for hp–adaptive finite element methods*. Submitted for publication, 2002.

[15] P. Houston and E. Süli, *Stabilized hp-finite element approximation of partial differential equations with non-negative characteristic form,* Computing, 66:99–119, 2001.

[16] P. Houston and E. Süli, *hp–Adaptive discontinuous Galerkin finite element methods for hyperbolic problems*. SIAM J. Sci. Comp., 23:1225–1251, 2001.

[17] M.G. Larson and T.J. Barth, *A posteriori error estimation for discontinuous Galerkin approximations of hyperbolic systems*. In: B. Cockburn, G. Karniadakis, and C.-W. Shu (eds.) Discontinuous Galerkin Finite Element Methods. Lecture Notes in Computational Science and Engineering, **11**. Springer, 2000.

[18] J. Nitsche, *Über ein Variationsprinzip zur Lösung von Dirichlet-Problemen bei Verwendung von Teilräumen, die keinen Randbedingungen unterworfen sind*. Abh. Math. Sem. Univ. Hamburg, 36:9–15, 1971.

[19] J.T. Oden, I. Babuška and C. Baumann, *A discontinuous hp–FEM for diffusion problems,* J. Comput. Phys., 146 (1998), pp. 491–519.

[20] O.A. Oleinik and E.V. Radkevič, *Second Order Equations with Nonnegative Characteristic Form*. American Mathematical Society, Providence, R.I., 1973.

[21] S. Prudhomme, F. Pascal, J.T. Oden and A. Romkes, *Review of* a priori *error estimation for discontinuous Galerkin methods*. TICAM Report 00–27, Texas Institute for Computational and Applied Mathematics, 2000.

[22] W.H. Reed and T.R. Hill, *Triangular Mesh Methods for the Neutron Transport Equation*. Technical Report LA-UR-73-479, Los Alamos Scientific Laboratory, Los Alamos, NM, 1973.

[23] B. Rivière and M.F. Wheeler, *A posteriori error estimates and mesh adaptation strategy for discontinuous Galerkin methods applied to diffusion problems*. TICAM Report 00–10, Texas Institute for Computational and Applied Mathematics, 2000.

[24] Ch. Schwab, *p- and hp-Finite Element Methods. Theory and Applications to Solid and Fluid Mechanics*. Oxford University Press, 1998.

[25] E. Süli and P. Houston, *Adaptive Finite Element Approximation of Hyperbolic Problems*. In T. Barth and H. Deconinck, editors, *Error Estimation and Adaptive Discretization Methods in Computational Fluid Dynamics*. Lecture Notes in Computational Science and Engineering, Volume 25, pp. 269-344, Springer–Verlag, 2002.

[26] E. Süli, P. Houston and Ch. Schwab, *hp–Finite element methods for hyperbolic problems*. In: J. R. Whiteman, editor, The Mathematics of Finite Elements and Applications X. MAFELAP 1999. Elsevier, 143–162, 2000.

[27] E. Süli, Ch. Schwab and P. Houston, *hp–DGFEM for Partial Differential Equations with Nonnegative Characteristic Form*. In: B. Cockburn, G. Karniadakis, and C.-W. Shu, editors, *Discontinuous Galerkin Finite Element Methods*. Lecture Notes in Computational Science and Engineering, Volume 11, pp. 221–230. Springer–Verlag 2000.

University of Oxford, Computing Laboratory, Wolfson Building,
Parks Road, Oxford OX1 3QD, UK
E-mail address: kathh@comlab.ox.ac.uk
E-mail address: endre@comlab.ox.ac.uk

Department of Mathematics & Computer Science, University of Leicester,
Leicester LE1 7RH, UK
E-mail address: Paul.Houston@mcs.le.ac.uk
E-mail address: W.Senior@mcs.le.ac.uk